PERFORMANCE OF LANTHANIDE-HALIDE SCINTILLATION DETECTORS IN PROMPT GAMMA ANALYSIS OF BULK SAMPLES

BY

MOHAMMAD SALEH AL-ANEZI

A Thesis Presented to the
DEANSHIP OF GRADUATE STUDIES

KING FAHD UNIVERSITY OF PETROLEUM & MINERALS

DHAHRAN, SAUDI ARABIA

In Partial Fulfillment of the
Requirements for the Degree of

MASTER OF SCIENCE

In

PHYSICS

August 2012

KING FAHD UNIVERSITY OF PETROLEUM & MINERALS
DHAHRAN 31261, SAUDI ARABIA

DEANSHIP OF GRADUATE STUDIES

This thesis, written by **Mohammad Saleh AlAnezi** under the direction of his thesis advisor and approved by his thesis committee, has been presented to and accepted by the Dean of Graduate Studies, in partial fulfilment of the requirements for the degree of **MASTER OF SCIENCE IN PHYSICS.**

Thesis Committee

June 09, 2012
Prof. Akhtar A. Naqvi (Chairman)

Dr. Muhammad A. Garwan (Member)

9th June, 2012
Prof. Anvarhusien A. Isab (Member)

Department Chairman
Dr. Abdul-Aziz Al-Jalal

29/5/2012
Dr. Mohamed S. Abdelmonem (Member)

Dean of Graduate Studies
Dr. Salam A. Zummo

10/6/12
Dr. Saleh I. Alquraishi (Member)

8/8/12
Date

DEDICATION

This thesis is dedicated to my wife **‘um Nasser’** without whose patience and support I would not have been able to persevere in this task

ACKNOWLEDGMENT

Praise to Allah the most gracious, the most merciful for whom has granted us existence and whom is the source of every success.

I would like to express my sincere gratitude to my advisor Prof. Akhtar Naqvi who was abundantly helpful and offered invaluable assistance, support and guidance. His guidance helped me in all the time of research and writing of this thesis. Without whose knowledge and assistance this study would not have been successful. Besides my advisor, I am extremely grateful to the thesis committee members: Dr.Muhammad A. Garawan, Prof. Anvarhusien A. Isab, Dr.Mohamed S. Abdelmonem and Dr.Saleh I. AlQurishi for their kindness in providing me with invaluable comments and recommendations for improvement.

Special thanks to the accelerator laboratory people: Mr.Raashid Muhammad and Mr.Abdul-Qadeer Khokhar. Acknowledgment is also owed to Mr.Khateeb-Ur-Rehman for helping me in the MCNP Code calculations. I would like to thank my graduate friends, Esam Al-Nahari, Abdul-Majeed Yahya, Qasim Darmosh and Muhammad Saleem for their various forms of support during my graduate study. Finally, acknowledgement is also due to King Fahd University of Petroleum and Minerals for providing the financial means and facilities in carrying out this work.

TABLE OF CONTENTS

LIST OF TABLES

TABLE **Page**

LIST OF FIGURES

FIGURE **Page**

THESIS ABSTRACT

Student's Name: Mohammad Saleh Al-Anezi

Title of Study: Performance of Lanthanide-Halide Scintillation Detectors in Prompt Gamma Analysis of Bulk Samples

Major Field: Physics

Date of Degree: August 2012

Performance tests of cylindrical 3" x 3" ($LaBr_3$:Ce and $LaCl_3$:Ce) and 5" x 5" (BGO) detectors were carried out to detect low energy prompt gamma-rays from boron contaminated water samples using a newly designed portable neutron generator-based Prompt Gamma Neutron Activation Analysis (PGNAA) setup. Prompt gamma-rays were measured from water samples contaminated with 0.031 to 0.5 wt% boron. The experimental yield of boron prompt gamma-rays measured with $LaBr_3$:Ce, $LaCl_3$:Ce and BGO detectors based PGNAA setup were compared. An excellent agreement has been observed between the experimental and calculated yield of boron prompt gamma ray from water samples. Minimum detection concentrations (MDC)s of boron in water samples for $LaBr_3$:Ce, $LaCl_3$:Ce and BGO detectors were determined to be: 30 ± 9.3, 45 ± 16.4, 28 ± 8 (ppm) respecteviley which agree with each other within statistical uncertainty.

خلاصة الرسالة

اسم الطالب: محمد صالح العنزي

عنوان الرسالة: أداء كواشف هاليدات اللانثانيد الوميضية في تحليل أشعة جاما الفورية

التخصص: فيزياء

التاريخ: أغسطس 2012

تم إختبار أداء كواشف أشعة جاما، ذات الأشكال الأسطوانية، التالية: ($LaBr_3$:Ce 3" x 3")، ($LaCl_3$:Ce 3" x 3") و (BGO 5" x5") من خلال الكشف عن أشعة جاما الفورية ذات الطاقة المنخفضة والمنبعثة من مادة البورون في عينات الماء وذلك بإستخدام التصميم الحديث لتقنية تحليل أشعة جاما الفورية بالتنشيط النيوتروني (PGNAA). تم اسنخدام عينات ماء تحتوي على تراكيز تتراوح من 0.031 إلى 0.500 نسب وزنية مؤوية من البورون. وقد تم مقارنة النتائج التجريبية لأشعة جاما الفورية ذات الطاقة 478 keV المنبعة من أسر النيوترونات الحرارية بواسطة البورون في عينات الماء والمقاسة بواسطة الكواشف الثلاث مع نتائج حسابات مونت كارلو. وقد لوحظ توافقٌ ممتاز بين النتائج العملية و النظرية لنفس الطاقة. حد الكشف الأدنى (MDC) لتركيز البورون في عينات الماء للكواشف ($LaBr_3$:Ce)، ($LaCl_3$:Ce) و (BGO) المؤسسة لتقنية (PGNAA) قد تم حسابه حيث كانت القيم: 9.3±30، 16.4± 45 و 8±28 جزء بالمليون (ppm) لكل كاشف على التوال

CHAPTER ONE

INTRODUCTION

Neutron activation analysis (NAA) is a popular technique to determine the concentration of trace and major elements in a vast amount of materials [1 & 2]. Prompt Gamma Neutron Activation Analysis (PGNAA) technique, which is a part of NAA technique, is used for online analysis. The performance of the PGNAA setup particularly detection limit depends upon gamma ray detector properties such as detector efficiency and energy resolution. The later property limits the detection sensitivity to those gamma rays which can be resolved by the detector. Sodium iodide NaI(Tl) and bismuth germinate (BGO) detectors have a typical energy resolution of 7 % and 11 % respectively for 662 keV gamma rays from ^{137}Cs source. New generation of lanthanum halide ($LaCl_3$:Ce and $LaBr_3$:Ce) scintillator detectors offer a very good energy resolution, energy linearity response, high light output, fast time response and good stopping power [3-7]. $LaBr_3$:Ce and $LaCl_3$:Ce are also more sensitive to gamma-rays than NaI and BGO detectors, due to their higher density [8]. Recently lanthanide-halides detectors have become commercially available in large crystal size. Cylindrical $LaBr_3$:Ce and $LaCl_3$:Ce detectors of 3 inches x 3 inches (Diameter x height) have energy resolution of 3 % and 4 % respectively for 662 keV gamma rays from ^{137}Cs source [9, 10]. The shortcoming of $LaBr_3$:Ce and $LaCl_3$:Ce

scintillators are their intrinsic activity lines, which appears as background spectral lines in their pulse height spectra. The intrinsic activity is due to the activity of the unstable ^{138}La isotope and uranium and actinium series contaminant present in these detectors [11, 12]. It is expected that PGNAA setup employing lanthanides-halide detectors will have improved gamma ray detection efficiency as compared to the employing NaI and BGO detectors.

1.1 Prompt Gamma-Ray Neutron Activation Analysis (PGNAA) technique

In NAA method, a sample is bombarded with neutrons, then neutrons interact with atoms in the sample to create new radioactive isotopes. As these radioactive nuclides decay, they emit gamma rays whose energies are characteristic for each nuclide. By measuring the gamma rays released when these isotopes decay, it is possible to determine which elements are present and their concentrations by comparison of the intensities of these gamma rays [2]. NAA thechnique is devided into two branches, with respect to a major experimental parameter; whether nuclear decay products (gamma rays) are measured during neutron irradiation (prompt gamma), or at some time after irradiation (delayed gamma), see Figure 1.1. In the PGNAA technique, a material is irradiated with fast neutrons [13]. Some of the fast neutrons are moderated by the material in an external moderator. These neutrons interact with the material through neutron inelastic scattering (n, n`$\gamma$) or thermal neutron capture ($n_{th}$, $\gamma$) reactions to produce prompt $\gamma$-rays. The elemental composition of the sample can then be determined from the intensity of prompt $\gamma$-rays produced, either through neutron inelastic scattering (n, n`γ) or thermal neutron

capture (n_{th}, γ) or both. Figure 1.2 shows prompt gamma rays energies due to inelastic scattering of neutrons from C, N and O elements.

There are some advantages in choosing the prompt γ-rays produced by thermal neutron capture for elemental analysis [14, 15]. The prompt γ-rays, due to thermal neutron capture, have generally higher energy as compared to those from neutron inelastic scattering. Accordingly, it is easier to detect higher energy thermal capture γ-rays. Prompt gamma-ray neutron activation analysis (PGNAA) is a non-destructive nuclear technique and is widely used for identification and quantification of elements in bulk gas, liquid, or solid samples [16-22]. PGNAA was developed for detection of concealed explosives in airline luggage during the late 1980s and is now being investigated and tested for new applications. These applications include detection of drugs in passenger luggage, detection of explosives and drugs in small packages, detection of liquid explosives in bottles, and detection of buried land mines and unexploded ordnance. For explosive, the PGNAA is based on the 10.8 MeV capture gamma ray from nitrogen, whose high density is uniquely characteristic of modern high explosives. For detection of drugs, the use of capture gamma ray signals from both hydrogen and chlorine (from hydrochloride drug salt) have been investigated, and a specific set of features based on these gamma ray signals selected for the detection algorithm [14, 15]. The technique is ideally suited for determination of elements concentration such as carbon, boron, chlorine, cadmium, oxygen, nitrogen… etc in bulk samples [16-20].

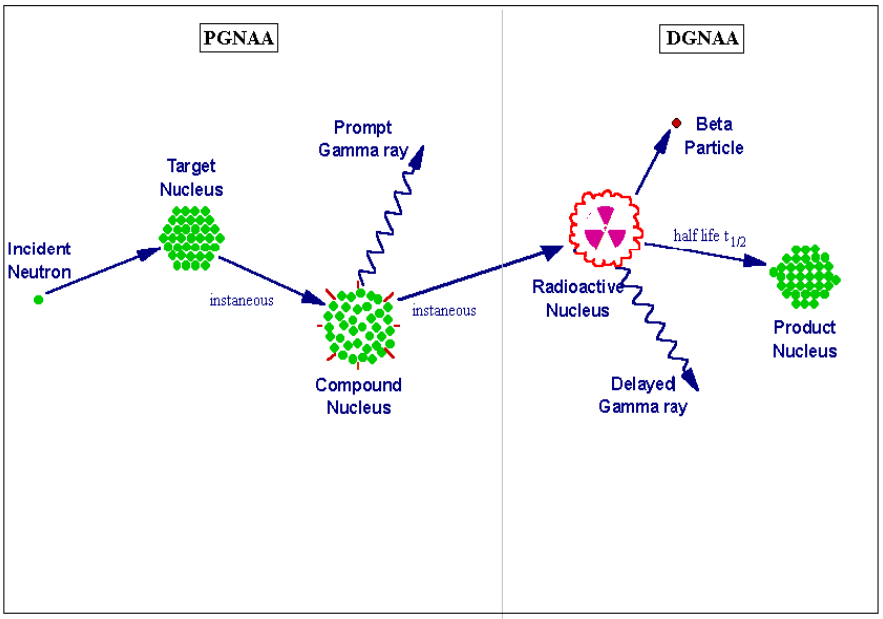

Figure 1.1 Schematic diagram illustrating neuclear decay products, prompt and delayed gamma ray

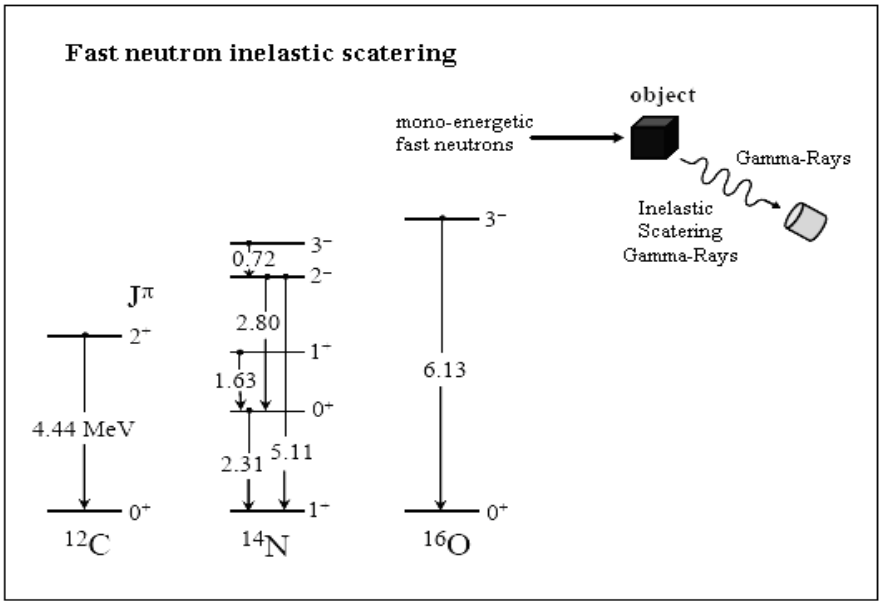

Figure 1.2 Gamma Ray decay scheme from inelastic scattering of neutrons from C, N and O

1.2 Boron Thermal Neutron Capture Reaction

In this project, detectors tests were carried out by measuring boron concentration in water samples using prompt gamma-ray neutron activation analysis (PGNAA) setup. The cross section for boron capturing neutrons increases drastically with lower neutron energy, reaching to 3980 barn at thermal energy level (E_{th}= 0.025 eV). Boron has two stable isotopes, ^{10}B and ^{11}B with abundances of 19.6 % and 80.4 % respectively. Thermal neutron capture cross section for ^{10}B is 3835 barns while for ^{11}B is 0.0055 barns. For ^{10}B reaction proceed as per following relation, see Figure1.3 also.

$$^{10}B + n \rightarrow {}^{11}B^{*} \rightarrow {}^{7}Li^{*} + \alpha$$
$$\downarrow$$
$$^{7}Li + E\gamma\ (0.478\ MeV) \qquad \ldots\ldots\ldots\ldots\ldots\ldots\ldots\ldots\ldots\ldots\ldots\ldots\ (1.1)$$

α particles and ^{7}Li are emitted with 0.84 and 1.47 MeV energy respectively along with 0.478 MeV prompt γ rays .

As shown in Figure 1.4, the compound nucleus ^{11}B is produced in an exited state at 11.4542 MeV with $(3/2)^{-}$ spin.

According to the total angular momentum and parity selection rules of nuclear reactions, ^{11}B cannot decay to ground state of ^{11}B , therefore it decays to an α particles and ^{7}Li.

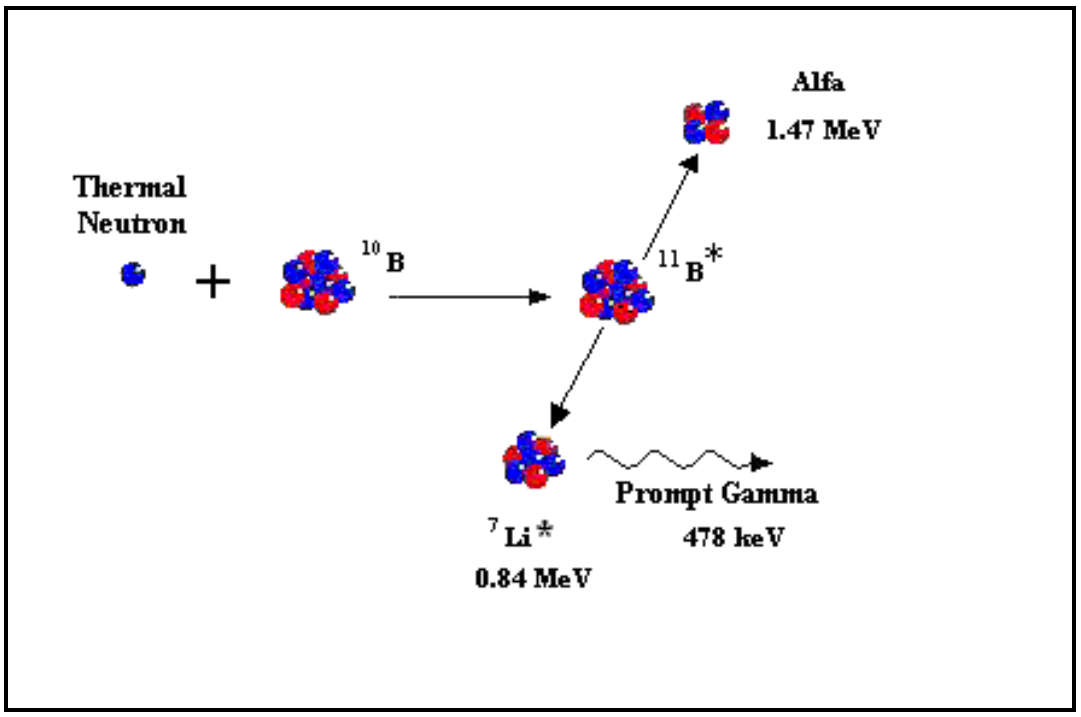

Figure 1.3 Schematic of the boron thermal neutron capture reaction [25]

1.3 Objectives

In this project it is proposed to design and test lanthanide-halide ($LaBr_3$:Ce and $LaCl_3$:Ce) detectors based prompt gamma-ray neutron activation analysis (PGNAA) setup for boron concentration measurements in water samples. Prompt gamma studies were carried out to measure prompt gamma ray yield from boron bulk samples with different concentration using lanthanide-halide detectors and BGO detectors. Results for the three detectors were compared.

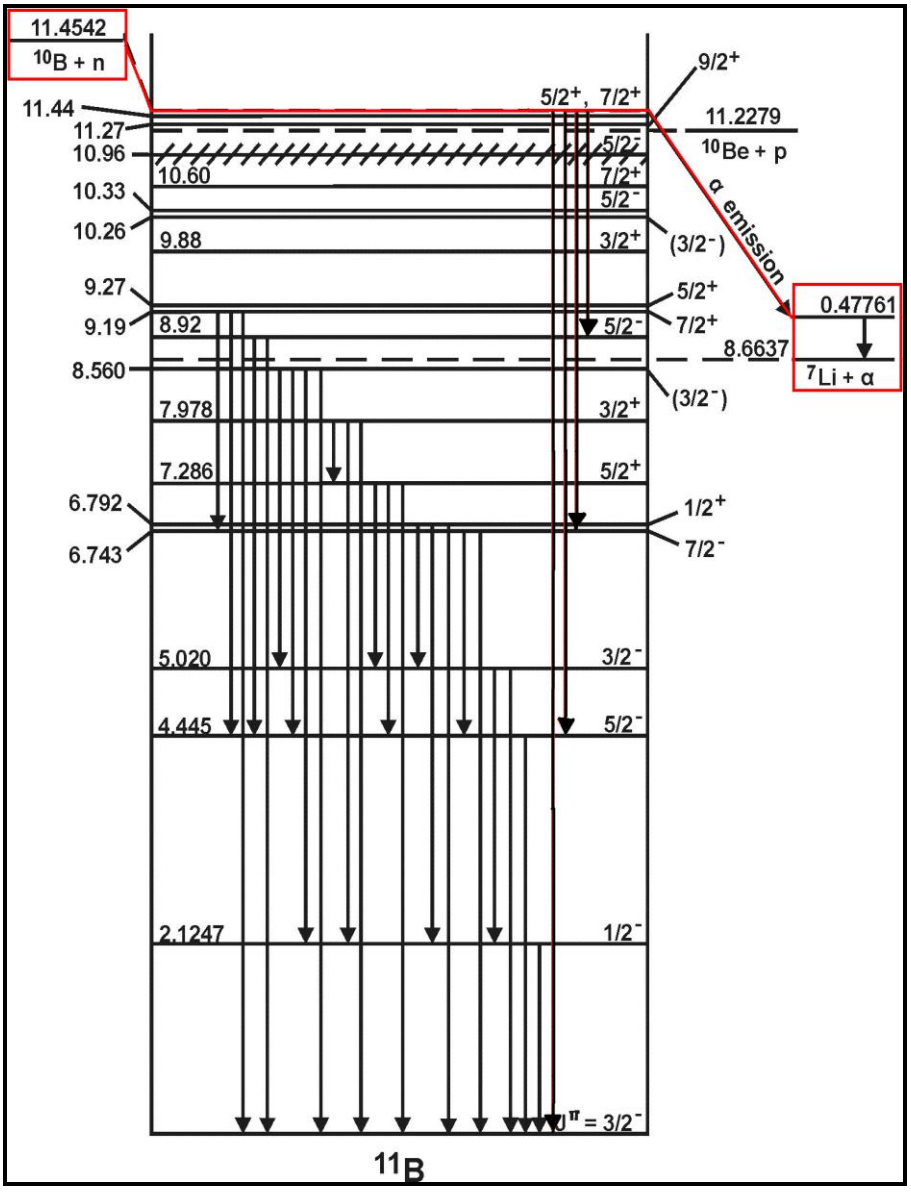

Figure 1.4 Level diagram of ^{11}B [52]

1.4 Literature Survey

The lanthanide-halides detectors are relatively a new generation of detectors, which there are no intensive studies in the field of prompt gamma ray neutron activation analysis by using these detectors. **A.Favalli et al. [26]** investigated the PGNAA using a 2"(diameter)x3"(length) $LaBr_3$:Ce scintillation detector. They compared the spectrum of NH4Cl taken with LaBr3:Ce detector and an HPGe planar detector. The results showed that the detector promises to be a suitable detector for the PGNAA application due to its excellent properties such as high energy resolution, high efficiency and elimination of cooling requirements [26].

A.Favalli et al. [27] also studied the full-energy peak efficiency of a 1.5 inch × 1.5 inch LaBr3:Ce scintillation detector in wide energy range of 200–5000 keV. In the energy range covered in their study, the full-energy peak efficiency exhibits a power law behavior. In comparison with a standard NaI(Tl) scintillation detector, the $LaBr_3$:Ce detector present a higher intrinsic efficiency for high-energy gamma rays. $LaBr_3$:Ce scintillation detector will be used in activation analysis in conjunction with the 14-MeV neutron generator and prompt gamma ray neutron activation analysis (PGNAA) technique [27].

T. Martinez et al. [28] have investigated the capabilities of the $LaCl_3$ and $LaBr_3$ scintillation materials for their use in measuring neutron capture reactions rates. They have determined experimentally the energy and time resolution, the intrinsic background of a 3"x3" $LaCl_3$ detector and calculated with GEANT4 simulations the neutron sensitivity of both materials. They have also investigated the neutron sensitivity of the $LaCl_3$ and $LaBr_3$ by GEANT4 Monte Carlo simulations and compared the results with

those of other scintillators commonly used for electromagnetism (EM) calorimeters. The neutron sensitivity was defined as the ratio of neutron reactions that have deposited in the calorimeter a total energy, *Esum,* more than 100 keV. At low neutron energies BGO offers the lowest neutron sensitivity, followed by BaF_2. However, it is interesting to notice that the values of $LaCl_3$ become close to those of BGO and clearly lower than those of BaF_2 at high neutron energies. NaI and $LaBr_3$ show larger neutron sensitivity than the rest of scintillators in the complete energy range. The results and their comparison with those of other scintillation materials indicate that $LaCl_3$ offers low neutron sensitivity in the keV region.

E. H. Seabury et al. [29] measured the response of a 2"x2" $LaBr_3$:Ce detector to multi-MeV gamma rays produced through neutron interactions on chlorine, hydrogen, iron, nitrogen, phosphorous, and sulfur. They also compared response of the $LaBr_3$:Ce detector to a 5"x5" NaI(Tl) detector an HPGe semiconductor detector. The $LaBr_3$:Ce detector has excellent energy resolution in all energy regions of the spectra when compared with NaI. As expected, the resolution is approximately a factor of ten worse than that of the HPGe semiconductor detector. The energy resolution, combined with its high efficiency and lack of a need for liquid-nitrogen cooling, make it a very good prospect for PGNAA applications.

John E. McFee et al. [30] studied the performance of large sizes 7.62 cm x7.62 cm $LaCl_3$ and $LaBr_3$ detectors with that of 7.62 cm by 7.62 cm cylindrical NaI(Tl) detector. An experimental investigation was undertaken to compare $LaCl_3$ and $LaBr_3$ detectors to NaI(Tl) with respect to parameters relevant to PGNAA landmine detection, including efficiency, energy resolution, linearity, available size and cost. They observed that larger $LaCl_3$ and $LaBr_3$ crystals do not exhibit such self-activity, as compared to the small size.

The advantages for PGNAA technique are immediately apparent in the 9.5–11 MeV region, where the triplet due to the 10.829 MeV nitrogen capture gamma ray is clearly resolved for LaBr, whereas it is barely resolved for NaI(Tl). The energy resolution of the 7.62Xcm7.62cm $LaBr_3$ is better than NaI(Tl) essentially at all energies and it is substantially better in the 9.5 to 11 MeV region. At the moderate count rates of these experiments, LaBr and LaCl are sufficiently linear for PGNAA purposes.

Lanthanum halide detectors, $LaBr_3$:Ce and $LaCl_3$:Ce, are available commercially in sizes up to 3"x 3" [12]. The properties of the lanthanum halide detectors are depend upon the crystal size. $LaBr_3$:Ce and $LaCl_3$:Ce (which we have in this study) are new detectors and have not studied extensively in the field of PGNAA technique specially for large crystal sizes.

CHAPTER TWO

THEORETICAL BACKGROUND OF THERMAL NEUTRON CAPTURE

A wide range of neutron source facilities are used for the implementation of PGNAA that can be divided into two groups: one group uses thermal or cold neutrons from nuclear reactors, while the other group utilizes smaller mobile systems that involve moderated neutron. Among the many differences between the facilities, the neutron energy spectrum and the epithermal neutron fraction have an important influence on the measured capture rate. Inhomogeneous flux profile also affects the measurement. Precise measurements and standardization can only be achieved by investigating the impact of these effects from different facilities. Hence, in the present chapter, definition of nomenclature and a general formalism are reviewed in the context of k_o standardization.

2.1 Definitions and nomenclatures

2.1.1 prompt k_o factor

When elements in a sample are analyzed, composite nuclear constant (k_o factor) is appeared, and it is defined as the following [31-32]:

$$k_0 = \frac{P_x(E_{\gamma,x})}{P_c(E_{\gamma,c})} \cdot \frac{\sigma_{o,x}}{\sigma_{o,c}} \cdot \frac{\theta_x / M_x}{\theta_c / M_c} \qquad (2\text{-}1)$$

Where: x and c: analyzed and comparator elements respectively, θ: isotopic abundance, M: element atomic weight, $P(E_\gamma)$: absolute γ emission probability (γ rays emission per each neutron capture), E_γ: prompt gamma ray energy, σ_o: thermal neutron capture cross-section at velocity of 2200 ms^{-1}. Assuming that specific isotope, which captures the neutrons, will immediately decay by emitting gamma rays at Eγ energy.

2.1.2 Elemental cross Section

Neutron speed-dependent capture cross sections $\sigma_\gamma(v)$ and 2200 ms^{-1} values (σ_o) are defined for a nucleus of an isotope. The partial capture cross section for the nucleus ($\sigma_\gamma(E_\gamma)$), is defined by the product $P(E_\gamma)\sigma_o$. An elemental cross section is defined for practical convenience in terms of a sample with isotopic natural abundance. A partial elemental capture cross section for the element Z is defined by [33]:

$$\sigma_\gamma^z(E_\gamma) = \theta P(E_\gamma)\sigma_o \quad , \tag{2-2}$$

where the notation is the same as listed previously. This term is the cross section per elemental atom to produce a particular gamma-rays of energy Eγ from irradiation with thermal neutrons.

2.1.3 Effective capture cross section

Effective capture cross-section is defined as the averaged cross-section over the neutrons spectra, and it is given in the relation [33]:

$$<\sigma>=\frac{\int_o^\infty n(v)\sigma_\gamma(v)vdv}{\int_o^\infty n(v)vdv}, \tag{2-3}$$

where v is the neutron speed, n(v)dv is the number density of neutrons with speed between v and v+dv, $\sigma_\gamma(v)$ is the neutron speed-dependent capture cross section of the nuclide under consideration.

2.1.4 Thermal and Epithermal Flux

As a consequence of the importance of thermal neutrons in capture reaction and the very large differences in the spectral shape and the fraction of epithermal neutrons in different irradiation facilities, the neutron density per unit speed interval is split into thermal and epithermal components, $n(v)=n_{th}(v)+n_{ep}(v)$, where n_{th} (the integrated thermal neutron density) is given by: $n_{th=} \int_o^\infty n_{th}(v)dv = n_{th} \int_o^\infty \rho_M(v)dv$, and $\rho_M(v)$ is the normalized Maxwellian function. The widely used definition in activation analysis is the 'conventional' thermal flux given by [34]:

$$\phi_{th}=n_{th}v_o \ , \tag{2-4}$$

The average thermal flux is the most convenient in reactor physics calculations, which is given by:

$$F_{th=} \int_o^\infty n_{th}(v)vdv = n_{th} \int_o^\infty \rho_M(v)vdv = n_{th}\bar{v} \tag{2-5}$$

Where $\bar{v}$ represents speed average in Maxwell distribution, and the ratio between the two fluxes is given by $F_{th}/\phi_{th=} \bar{v}/v_o=(4T/\pi T_o)^{1/2}$, where T represents the temperature and To = 293.6 K is the Maxwell's temperature. The neutron flux φ_{ep} is more convenient in the case of epithermal neutrons, and represents the product of neutron speed and density ($\varphi_{ep} = vn_{ep}$). This approach describes the neutron flux spectrum in terms of energy, and is based

on theoretical considerations that ideally the distribution follows 1/E shape [34]. The relationship between epithermal neutrons density and the flux is:

$$n_{ep}(\nu)\, \nu\, d\, \nu = \varphi_{ep}(E)dE = \phi_{ep}\, dE/E \qquad (2\text{-}6)$$

2.1.5 Westcott g-factor

Reactor neutron capture and fission reaction rates are determined as the product of the neutron flux density and the neutron capture or fission cross section. The standard energy for tabulation of thermal neutron cross sections is that of room temperature of 20.43^{o} C, corresponding to a neutron energy of 0.0253 eV or a neutron velocity of 2200 ms^{-1}. Since most reactions do not operate at a temperature of 20^{o} C, there must be some mechanism for converting the cross section, σ_o, at the tabulated energy to the effective cross section, σ, at the actual temperature of the reactor [35]. Westcott developed a method for converting a σ_o to σ by describing the neutron spectrum as a combination of a Maxwell-Boltzmann speed distribution function which is characterized by a temperature T and component of epithermal energy neutrons, whose neutron flux density distribution is proportional to the reciprocal of the neutron energy, i.e., dE/E. For an isotope whose neutron capture cross section does not vary inversely with the neutron velocity, $\hat{\sigma} = \sigma_0 (g_w + rs)$ where g is the Westcott g-factor, the epithermal index, r, is approximately the fraction of the total neutron density in the epithermal component, and s is a temperature dependent quantity related to the reduced resonance intern. In the absence of an epithermal component, r = 0, and the g-factor is the ratio of the Maxwellian averaged cross section to the 2200 m/s cross section, σ_o. So,

$$g_w(T) = \frac{\hat{\sigma}_M(T)}{\sigma_o} = \frac{1}{\sigma_o v_o}\int_o^\infty \rho_M(v,T)\sigma_\gamma(v)v\,dv$$

$$= \frac{1}{\sigma_o v_o}\int_o^\infty \frac{4}{\sqrt{\pi}}\left(\frac{v}{v_T}\right)^3 e^{-(v/v_T)^2}\sigma_\gamma(v)\,dv \qquad (2\text{-}7)$$

Where v_T, the speed maximum value in Maxwellian function, which is related with temperature (T) by: $mv_T^2/2 = kT$ or $v_T = v_o(T/T_o)^{1/2}$. If σ(v) varies as l/v, the Maxwellian cross section is equivalent to the 2200 m/s value and g = 1. For nuclides with resonances in the thermal neutron energy range, g-factors are different from unity and g-factors will be temperature dependent [35].

2.2 General Formats

2.2.1 Capture rate

The instantaneous neutron capture rate dR(t) of a stable nuclide in differential volume d^3r localized at r of a sample in a neutron field is given by :

$$dR(t) = d^3\mathbf{r}\; n_x(\mathbf{r}) \int_o^\infty n(\mathbf{r},v,t)\sigma_r(v)v\,dv \qquad (2\text{-}8)$$

Where: $n_x(r)$: capturing nuclei density at target sample, n(**r**,v,t): neutron density per speed period at **r** position and time t. For nuclei that subject to $\frac{1}{v}$, with homogeneous nuclide density, the time-averaged capture rate in the sample is given by [32]:

$$\langle R\rangle_{1/v} = \frac{1}{V}\frac{m}{M}N_A\theta\int_v d^3\mathbf{r} \int_o^\infty n(\mathbf{r},v)\sigma_\gamma(v)v\,dv = \frac{m}{M}N_A\theta\sigma_o v_o \bar{n}_t \qquad (2\text{-}9)$$

Where: V: sample's volume, m: the mass of the target element, M: the element's atomic mass, N_A: Avogadro's number, θ: the abundance of the isotope, which does the capture

process in the element, n(**r**,v): time-averaged neutron density per speed interval unit at *r* position, n_t : volume –averaged total neutron density in the sample. The result is exact even when the spectrum in the sample is distorted or the neutron beam profile is inhomogeneous.

2.2.2 Non-1/v absorber, effective g-factor and Cd ratio

The capture rate for a non-1/v absorber has been quantified in terms of the Westcott g-factor. As the g-factor is defined for a Maxwellian thermal spectrum, one is faced with the problem of treating realistic neutron spectra, which may deviate significantly from the Maxwellian shape in the thermal energy region. Furthermore, the thermal spectrum deviates from Maxwellian in filtered beam facilities, where the spectrum form is distinctly non Maxwellian [33]. As the capture rate for a non-1/v absorber is highly dependent on the shape of the thermal and epithermal spectrum, a generalized approach is described in terms of an effective g-factor. The neutron energy [E_{Cd}=0.5 eV] taken as the boundary between those low energy neutrons that are absorbed by cadmium sheet and those higher energy neutrons that are not so absorbed. The non-1/v capture rate in terms of effective g-factor and cadmium ratio is given by:

$$\langle R \rangle_{non-1/v} = \frac{m}{M} N_A \theta \bar{n}_{th} v_o \hat{g} \sigma_o \left(\frac{R_{Cd}}{R_{Cd} - 1} \right) \tag{2-10}$$

While the effective g-factor and cadmium ration are given by [36]:

$$\hat{g} = \frac{1}{\sigma_o v_o} \frac{\int_o^{v_{Cd}} \rho_{th}(v) \sigma_\gamma(v) v dv}{\int_o^{v_{Cd}} \rho_{th}(v) dv} = \frac{1}{\sigma_o v_o} \int_o^{v_{Cd}} \rho_{th}(v) \sigma_\gamma(v) v dv \,, \quad \text{and}$$

$$R_{Cd} = 1 + \frac{\bar{n}_{th} v_o \hat{g} \sigma_o}{\bar{n}_{ep} \int_{v_{Cd}}^{\infty} \rho_{ep}(v) \sigma_\gamma(v) v dv}.$$

$\rho_{th}(v)$ and $\rho_{ep}(v)$ are thermal and epithermal neutron speed distribution functions. $\bar{n}_{ep}$ and $\bar{n}_{th}$ represent the average size of neutrons density for each thermal and epithermal neutrons in the sample.

2.2.3 Prompt Capture-Gamma Rays Counting Rate

The measured count rate of a prompt gamma ray of energy E_γ emitted from a capturing nuclide is given by:

$$\langle C \rangle = \frac{1}{V} \frac{m}{M} N_A \theta \int_V d^3\mathbf{r} \quad \varepsilon(\mathbf{r}, E_\gamma) \int_o^{\infty} p(E_\gamma v) n(\mathbf{r}, v) \sigma_\gamma(v) v dv \tag{2-11}$$

where $\varepsilon(\mathbf{r}, E_\gamma)$ is the detection efficiency for the prompt gamma rays of energy E_γ emitted at location r, and $P(E_\gamma, v)$ is the absolute gamma-ray emission probability (gammas emitted per capture) of the prompt gamma ray of energy E_γ emitted from the nucleus capturing a neutron of speed v. Detector specifications and the sample geometrical factors affect on $\langle C \rangle$ value. For slow neutron capture, $P(E_\gamma, v)$ is assumed to be independent of. By combining Equations (2-10) and (2-11), the specific count rate (per mass of element in the sample, or the so-called analytic sensitivity) is given by [33]:

$$A = \left\langle \frac{C}{m} \right\rangle = \frac{N_A}{M} \theta P(E_\gamma) \varepsilon(E_\gamma) \bar{n}_{th} v_o \hat{g} \sigma_o \left(\frac{R_{Cd}}{R_{Cd} - 1} \right) \tag{2-12}$$

2.2.4 Experimental calculation of k_o factor

The same irradiation conditions for analyte (x) and comparator (c) elements are achieved by co-irradiating a homogeneous mixture of analyte and comparator element in a neutron

field, and measuring the signature of prompt gamma rays in parallel. Hence, the experimental prompt k_0 factor is given from Equations (2-1) and (2-12) by [33]:

$$k_o = \frac{P_x(E_{\gamma,x})}{P_c(E_{\gamma,c})} \cdot \frac{\sigma_{o,x}}{\sigma_{o,c}} \cdot \frac{\theta_x / M_x}{\theta_c / M_c} = \frac{A_x / \varepsilon(E_{\gamma,x})}{A_c / \varepsilon(E_{\gamma,c})} \cdot \frac{\hat{g}_c}{\hat{g}_x} \cdot \frac{\left(\frac{R_{Cd}}{R_{Cd}-1}\right)_c}{\left(\frac{R_{Cd}}{R_{Cd}-1}\right)_x} \qquad (2\text{-}13)$$

This general expression contains two correction factors: ĝ for non-1/v absorption, and R_{Cd} for epithermal absorption.

CHAPTER THREE

MCNP CODE FOR DESIGN A SETUP

3.1 Introduction

MCNP is a general expression meant to Monte Carlo N-Particle code. MCNP is a general-purpose, continuous-energy, generalized-geometry, time-dependent, coupled neutron/photon/electron modular Monte Carlo transport code. MCNP can be used in several transport modes: neutron only, photon only, electron only, combined neutron/photon transport where the photons are produced by neutron interactions, neutron/photon/electron, photon/electron, or electron/photon. The code can be used to design an experimental setup [37].

MCNP code requires experimental geometry, sample material, beam energy, reaction type, and particle energies whose intensity has to be recorded. To obtain the design statistics, one has to choose appropriates number of particle histories.

The yield of prompt gamma rays due to thermal neutron capture depends upon the concentration of the elements of interest in the sample as well as thermal neutron flux available at the position of the sample. Since the thermal neutrons are mainly produced through moderation of fast neutrons from an external moderator [38], production of maximum thermal neutron flux at the sample location requires optimization of the size of

that moderator. In addition, given that γ-ray yield of a specific element increase with sample size but is offset by increasing γ-ray attenuation, it is further clear that need exists for the sample size to be optimized. The performance of a PGNAA setup also depends upon sample parameters, such as bulk density and moisture content [39]. Also thermal neutron flux at the sample depends upon incident neutron energy as well as source moderator geometry, so changing the neutron source is one of the important parameter to be optimized. In summary, design calculations of a PGNAA setup are multi-factorial; in essence requiring a Monte Carlo simulation of neutron induced prompt γ -ray processes in the sample [38].

3.2 MCNP Input File

The neutron energy regime is from 10^{-11} MeV to 20MeV, and the photon and electron energy regimes are from l KeV to 1000MeV. The input file contains the information to describe the various part of setup design such as: i) geometry specification, ii) The Materials and their evaluated cross-section evaluations, iii) The location and characteristics of the neutron, photon, or electron source, iv) The type of answers or tallies desired, and any variance reduction techniques used to improve efficiency.

3.2.1 Experimental geometry specification

The geometry of MCNP treats an arbitrary three-dimensional configuration of user-defined materials in geometric cells bounded by first- and second-degree surfaces and fourth-degree elliptical tori. The cells are defined by the intersection, unions, and complements of the regions bounded by the surfaces. Surfaces are defined by supplying

coefficients to the analytic surface equations or, for certain types of surfaces, known points on the surfaces [37].

3.2.2 Material and Nuclear Cross-Section Data Library

MCNP uses continuous-energy nuclear and atomic data libraries. Over 500 neutron interaction tables are available for approximately 100 different isotopes and elements. Multiple tables for a single isotope are provided primarily because data have been derived from different evaluations, but also because of different temperature regimes and different processing tolerances. Photon interaction tables including coherent and incoherent scattering, photoelectric absorption exist for all element from Z=l through Z=94. Cross sections for nearly 2000 dosimetry or activation reactions involving over 400 target nuclei in ground states are part of the MCNP data package. Users may select specific data tables through unique identifiers for each table. The primary sources nuclear of nuclear data are taken from the Evaluated Nuclear Data Files (ENDF) system, the Evaluated Nuclear Data library (ENDL) and the Activation Library (ACTL) and collected from the Applied Nuclear Science (T-2) Group at Los Alamos.

3.2.3 Neutron and Gamma Source Specification

The program's user can specify different situations and wide range of source conditions without having to make a code modification. The source selection list in the input file is symbolized by SDEF, which is followed by some source parameter, such as position, energy, radiation type … etc [37].

3.2.4 Tallies and Output

Tallies represent the digital record of the random events from neutron interaction with the sample elements. The user can instruct MCNP to make various tallies related to particle current, particle flux, and energy deposition. MCNP tallies are normalized to be per starting particle except for a few special cases with criticality sources.

3.2.5 Estimation of Monte Carlo Errors

MCNP tallies are normalized to be per starting particle and are printed in the output accompanied by a second number R, which is the estimated relative error defined to be one estimated standard deviation of the mean E_n divided by the estimated mean $\bar{x}$ or: $R = \frac{S_{\bar{x}}}{\bar{x}}$. In MCNP, the quantities required for this error estimate - the tally and its second moment - are computed after each complete Monte Carlo history, which accounts for the fact that the various contributions to a tally from the same history are correlated. For a well-behaved tally, R will be proportional to $1/\sqrt{N}$ where N is the number of histories. Thus, to halve R, we must increase the total number of histories fourfold. For a poorly behaved tally, R may increase as the number of histories increases. The quantity R should be less than 0.10 to produce generally reliable confidence intervals. For a given MCNP run, the computer consumed time T is proportional to N. Thus:

$R = C/\sqrt{T}$; where C is a positive constant. There are two ways to reduce R (estimated relative error): increase T and / or decrease C.

Computer budgets often limit the utility of the first approach. For example, if it has taken 2 hours to obtain R=0.10, then 200 hours will be required to obtain R=0.01. For this

reason MCNP has special variance reduction techniques for decreasing C. (Variance is the square of the standard deviation) the constant C depends on the tally choice and / or the sampling choices.

3.3 PGNAA Setup

The PGNAA setup is based on the portable neutron generator MP320, moderator, bulk sample and gamma ray detector. Figure 3.1 shows schematic of the PGNAA setup consisting of a hollow cylindrical moderator enclosing the bulk sample. Incident 2.5 MeV neutrons from the portable neutron generator is moderated to thermal energies in the walls of the moderator cylinder, which is made of high density polyethylene. The portable neutron generator views the moderator cylinder at right angle to its symmetry axis. The gamma ray detector surrounded by lead shielding and neutron shielding (containing of lithium carbonate mixed with paraffin wax), view the sample along the axis of cylindrical moderator. The optimum thickness of the cylindrical moderator, that can produce maximum yield of the prompt gamma-rays the detector location, has been calculated using Monte Carlo simulation code MCNP4B [40 & 41].

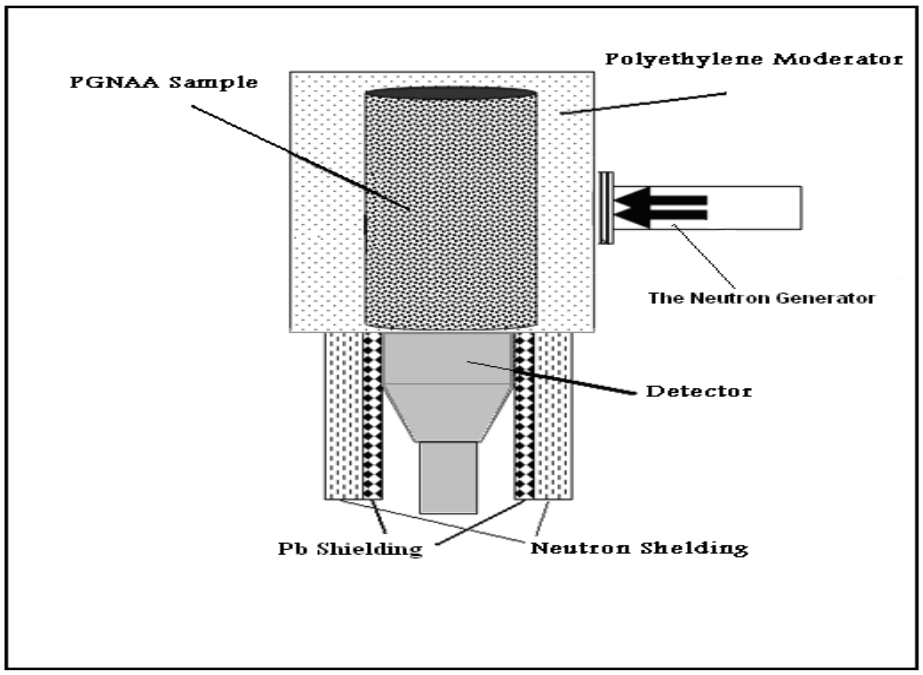

Figure 3.1 Schem6atic of PGNAA setup

3.4 Design Calculation of PGNAA Setup

Monte Carlo calculations were carried out using code MCNP4B2 to determine the optimum geometry of portable neutron generator based PGNAA setup utilizing thermal neutron capture reaction [37]. We have chosen a sample with a diameter of 9 cm and a length of 14 cm. The neutron generator is touching the moderator. We set, as experiment, the thicknesses of detector lead shielding and detector neutron shielding, 1 cm and 3 cm, respectively. The detector, as shown in Figure 3.1, is touching the sample and the moderator. In the present study, the optimum value of the moderator thickness will obtain to produce maximum yield of thermal neutron flux in the sample. The optimum value will obtain through calculated thermal neutron yield inside the moderator cavity with inner diameter of 9 cm (empty sample), as a function of the outer moderator diameter (moderator thickness). Figure 3.2 shows calculated thermal neutron yield inside the

moderator cavity with fixed inner diameter of 9 cm, as a function of moderator thickness. Thermal neutron yield inside the sample initially increases with moderator thickness up to 5 cm and then it exhibits yield saturation over a moderator thickness of 5 to 6 cm. With further increase in the moderator thickness, the yield drops off. The initial increase in the yield is due to increasing moderator thickness while the yield saturation with further increase in moderator thickness may be due to a balance between thermal neutron production and attenuation over the thickness of the moderator. The final drop in the yield is due to dominating thermal neutron attenuation effects over the moderator thickness. From the results of the calculations, the deduced optimum moderator thickness was 6 cm.

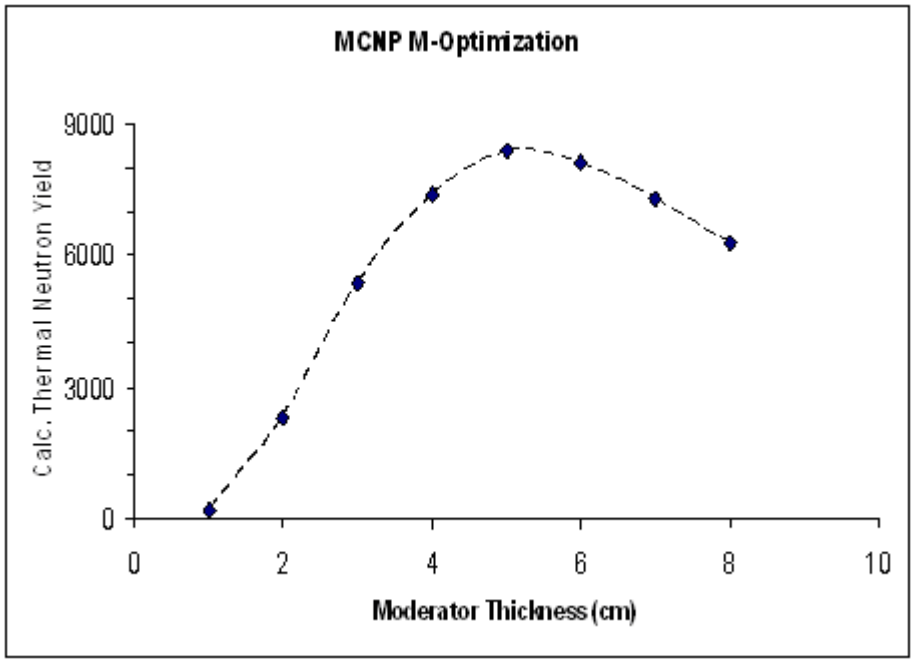

Figure 3.2 Calculated thermal neutron yield inside the sample (moderator cavity) plotted as a function of moderator thickness

3.5 Prompt Gamma-Rays Yield Calculation from Boron in Water Samples

Theoretical prompt gamma-rays produced from boron in water samples were obtained through Monte Carlo calculations. We used the same PGNAA design parameters described in section 3.5. We fill the sample by water, after that, the water sample was mixed with 0.03125 wt.% concentration of boron. Theoretical prompt gamma-rays yield from boron was calculated by applying 2.5 MeV neutron beam. The same steps were done for water samples containing 0.125, 0.250, 0.500 wt.% concentration of boron. Figure 3.3 shows the theoretical prompt gamma-rays yield obtained through Monte Carlo calculations.

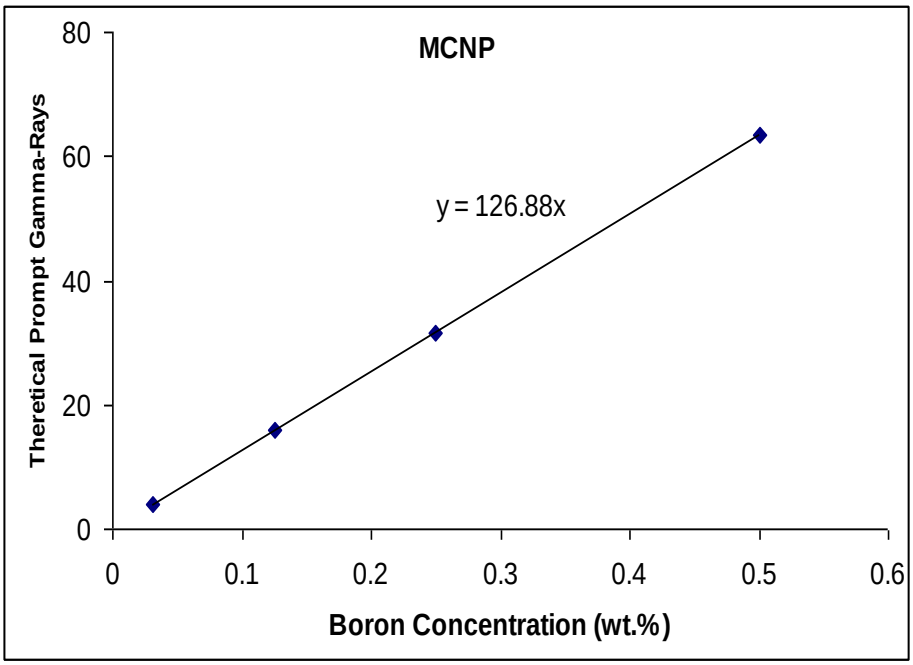

Figure 3.3 Theoretical prompt gamma-rays of 0.03125, 0.125, 0.250, 0.500 wt.% of boron in water concentration obtained through Monte Carlo calculations.

CHAPTER FOUR

FABRICATION AND PERFORMANCE TEST OF THE PORTABLE NEUTRON GENERATOR BASED PGNAA SETUP

Portable neutron generator based PGNAA setup consists of MP320 portable neutron generator; gamma-rays detector, lanthanum-halides or BGO detectors; moderator cylinder and the bulk sample. In this chapter, we will describe, and then, test the PGNAA setup [42, 43, 44].

4.1 Portable Neutron Generator based PGNAA Setup

Portable neutron generators are increasingly used in neutron activation field measurements. KFUPM has acquired a ThermoScientific® MP320 D(d,n) (Deuterium-Deuterium) reaction based 2.5 MeV portable neutron generator for its prompt gamma analysis programs. It is lightweight, about 10 kg, and suited for most demanding field or laboratory applications. Figure 4.1 shows a picture of MP320 portable neutron generator.

Table 4.1 shows some of the MP320 specifications [45]. Figures 4.2 and 4.3 show pictures of MP320 based PGNAA setup.

Figure 4.1: A picture of the MP320 portable neutron generator

Figure 4.2 A picture of the PGNAA setup top-view

TABLE 4.1 MP 320 Neutron Generator Specification Sheet [45]

MP320 Parameters	**Values**
Maximum neutron yield, n/s	$2x\ 10^6$
Rated neutron yield,* n/s	$>1x\ 10^6$
Time @ rated yield, hours	600
Pulse frequency range,	Hz 100–20,000
Pulse duty cycle range	5–100%
Pulse rise time, μs	Variable <1
Pulse fall time, μs	<1, <1
Minimum pulse width, μs	5
Operating high voltage, kV	45-75
Beam current, μA	25-80
Operating temperature range, °C	–25 to +50 0
Input power requirements	120/220 VAC (50–60 Hz)
Total system weight kg	12
Neutron generator weight, kg	10
Neutron generator physical dimension (Diameter x Length)	ϕ 12.1 cm x 57.2 cm

* Rated yield for D-D neutron MP320 generator

Figure 4.3 A picture of the PGNAA setup-side view

4.2 Performance Test of Portable Neutron Generator Based PGNAA Setup

Performance of a portable pulsed neutron generator model MP320 was evaluated experimentally for its application in Prompt Gamma Neutron Activation Analysis (PGNAA). The optimum operating high-voltage and beam current of the MP320 neutron generator to produce optimum neutron flux, was experimentally determined from prompt gamma ray yield measurement from an iron sample as a function of deuteron beam voltage and current. The efficacy tests of neutron flux the MP320 generator for its application in prompt gamma studies was carried out through chlorine prompt gamma ray yield measurements from water samples contaminated with 1.0 to 4.0 wt. % chlorine concentrations.

4.2.1 Measure of Gamma Ray Yield as a Function of Accelerator High Voltage and Beam Current

2.5 MeV neutrons can be produced from the generator using 45 to 75 kV deuteron beam voltage with 30 to 80 μA beam current. The optimum operating voltage and beam current of the MP320 neutron generator to produce optimum neutron flux will experimentally determine from prompt gamma ray yield measurement from an iron sample as a function of deuteron beam voltage and current. An iron sample was chosen because it has high-energy prompt gamma rays, which can be easily discriminated from low-energy room scattered inelastic gamma rays. A cylindrical iron sample, with 10 cm x 15.8 cm (diameter x height) dimensions, was placed in the moderator and was irradiated with 2.5 MeV neutron beam from the pulsed neutron generator. The neutron generator was operated at 250 Hz with 5 % duty cycle. Pulsed neutron beam improves signal to background ratio in the PGNAA studies. The prompt gamma-rays produced in the iron specimen were detected by a cylindrical 12.5 cm by 12.5 cm (diameter x length) bismuth germinate (BGO) detector. BGO detector was chosen to detect prompt gamma because of its higher resistance to neutron radiation damage [46]. The prompt gamma-ray yield data from iron sample were acquired as a function of deuteron beam energy and deuteron beam current. The prompt gamma ray yield data were taken for deuteron beam energy varying over 45, 50, 55, 60, 65 and 70 kV for deuteron beam voltage, and 30, 40, 50, 60 and 70 μA for deuteron beam current.

There are several prompt gamma rays emitted by iron due to capture of thermal neutron at 5.902, 6.018, 7.278, 7.631 and 7.645 MeV. Due to poor energy resolution of BGO detector (about 11 % energy resolution for 662 keV gamma rays from ^{137}Cs source) the

detector could not resolve between the gamma rays of energies 5.902 and 6.018 MeV as well as 7.631 and 7.645 MeV. The relative intensities of theses gamma rays are given in Table 4.2 [33]. During the irradiation of the Iron sample, the detector, although shielded was also exposed to thermal neutrons and it registered the prompt gamma rays due to capture of thermal neutrons in Bi and Pb elements present in the detector and gamma ray detector shielding respectively. These peaks were present in the Iron spectra and needed to be subtracted as beam associated background. Figure 4.4 shows beam associated background spectrum of the BGO detector operated at 45 kV and 70 μA. (4.054 and 4.171) MeV from Bi and 7.38 from Pb lines are appear in the spectra. Figure 4.5 shows pulse height spectra of prompt γ-rays spectrum of Iron sample taken at 45 kV operating accelerator voltage and 70 mA beam current. The main feature of Figure 4.5, is the presence of iron thermal neutron capture peaks at 5.902, 6.018, 7.631 and 7.645 MeV. Figure 4.6 shows enlarged prompt gamma experimental pulse height spectra from an iron sample taken with 45, 50, 55, 60, 65, 70 and 75 keV deuteron beam with 70 mA beam current. Also superimposed on the spectrum is background gamma ray spectrum.

TABLE 4.2 Energies and Partial Elemental Cross Section $\sigma_\gamma^z(E_\gamma)$-barns of Prominent Capture Gamma Rays of Iron and Chlorine [33]

Element	**Gamma-Rays Energy (MeV)**	**$\sigma_\gamma^z(E_\gamma)$-barns**
Fe	5.920	0.225
	6.018	0.227
	7.278	0.137
	7.631	0.653
	7.645	0.549
Cl	1.164	8.91
	1.951	6.33
	1.959	4.10
	2.863	1.82
	3.062	1.13
	4.98	1.23
	5.715	1.82
	6.110	6.59
	6.619	2.53
	6.627	1.47
	7.413	3.29
	7.790	2.66

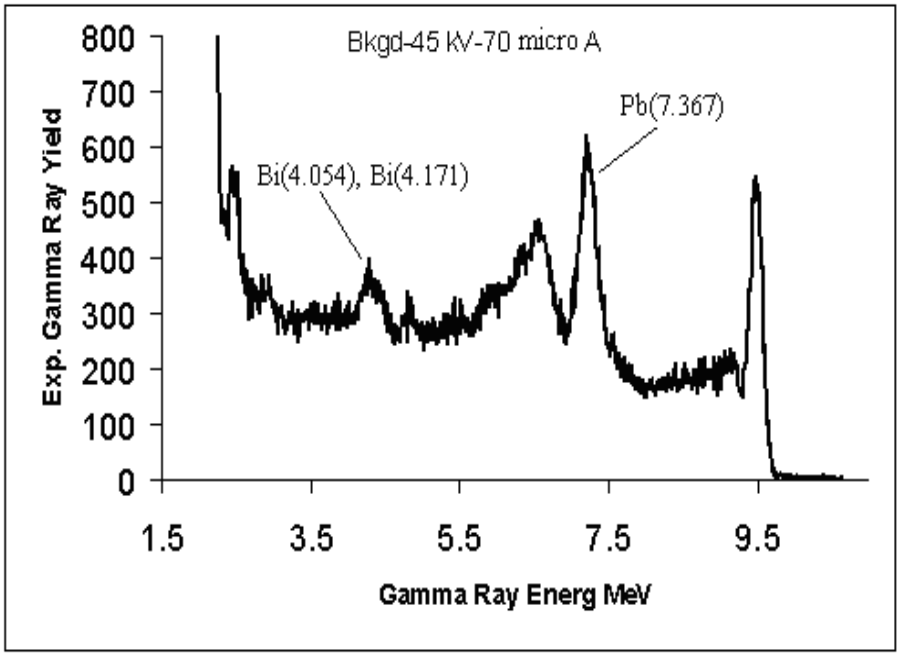

Figure 4.4 Background prompt gamma ray pulse height spectra of the BGO detector.

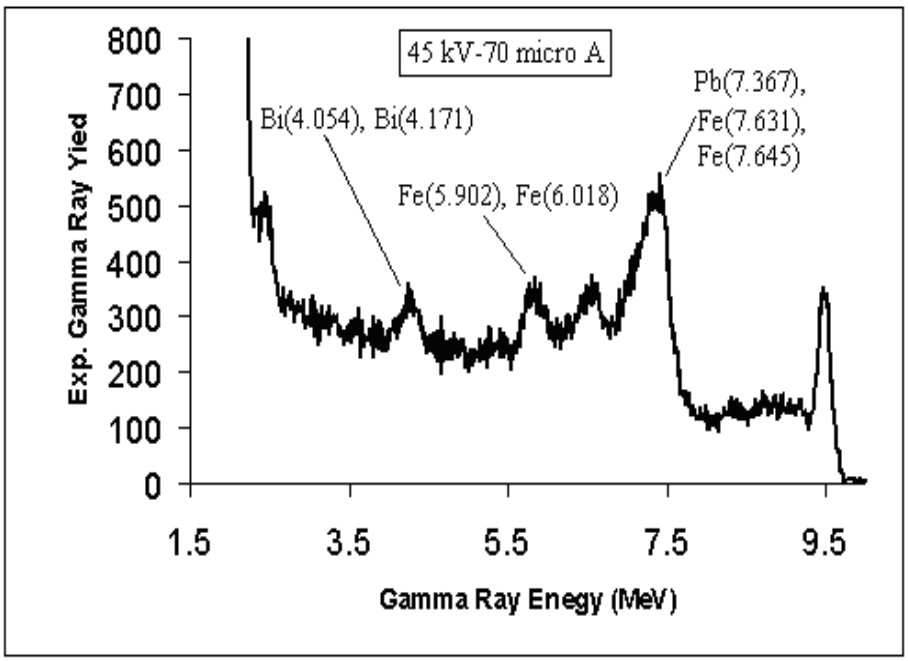

Figure 4.5 Prompt gamma ray pulse height spectra from Iron sample taken at 45 kV, 70 μA operating accelerator voltage and beam current.

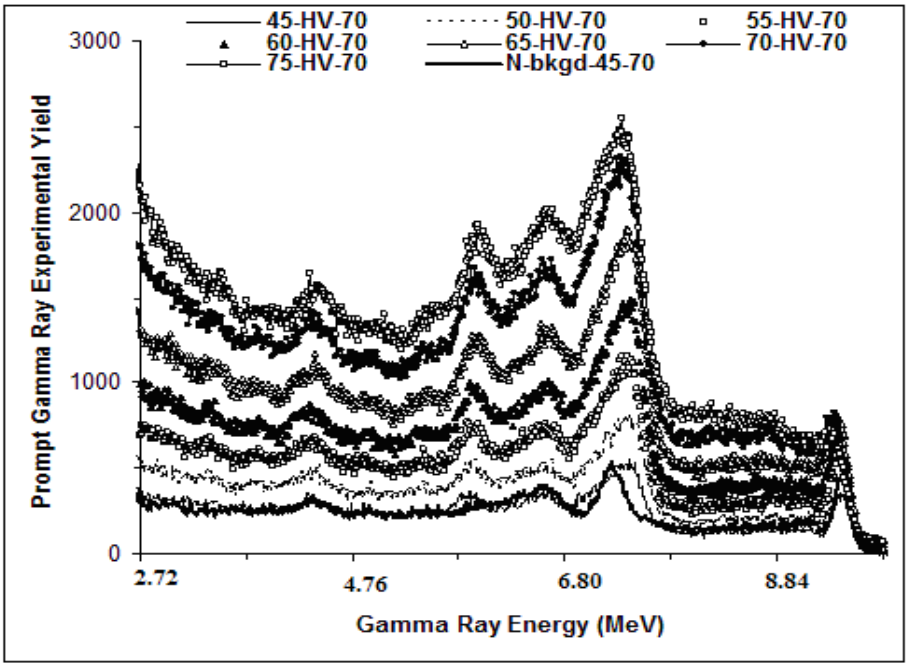

Figure 4.6 Enlarged prompt gamma ray spectra from an iron sample taken with several values of keV deuteron beam with 70 μA beam current.

Figure 4.7 shows the iron spectrum after background subtraction. The main feature of Fig. 4.7 is the increased intensity of iron peaks at 5.902 + 6.018 MeV. The iron gamma ray doublet at 7.631+ 7.645 MeV is interfering with prompt gamma peak from ^{207}Pb at 7.367 MeV present in the background spectrum, Figure 4.4. The full energy peak at 7.278 MeV from iron interferes with single escape peaks of iron doublet at 7.631+ 7.645 MeV as well as single escape peak of 7.367 MeV from ^{207}Pb. The prompt gamma ray peaks due to capture of thermal neutrons in Bi present in BGO detector appears at 4.171 and 4.054 MeV in all spectra. With increasing high voltage, the peak intensity increases in the spectra. In order to obtain the prompt gamma yield as a function of beam voltage, background spectra were subtracted from iron spectra. Fig. 4.7 shows the subtracted spectra of prompt gamma-ray from iron sample. Prominent prompt gamma-ray peak at 6.1, 7.2 and 7.6 MeV from iron are clearly shown in Fig. 4.7. Finally, counts under each

peak were integrated and normalized to the same amount of measurement time. Figure 4.8 shows the normalized experimental yield of 7.6 MeV prompt gamma rays from iron plotted as a function of deuteron beam current for 45, 50, 55, 60, 65 and 70 keV deuteron beams. The lines are drawn through the points to show the data trend. The yield of 7.6 MeV prompt gamma ray increases with increasing beam current as well as beam voltage. The optimum operating parameters of the MP320 neutron generator to produce maximum yield of prompt gamma ray yield were observed to be 70 kV deuteron beam voltage with 70 μA deuteron beam current.

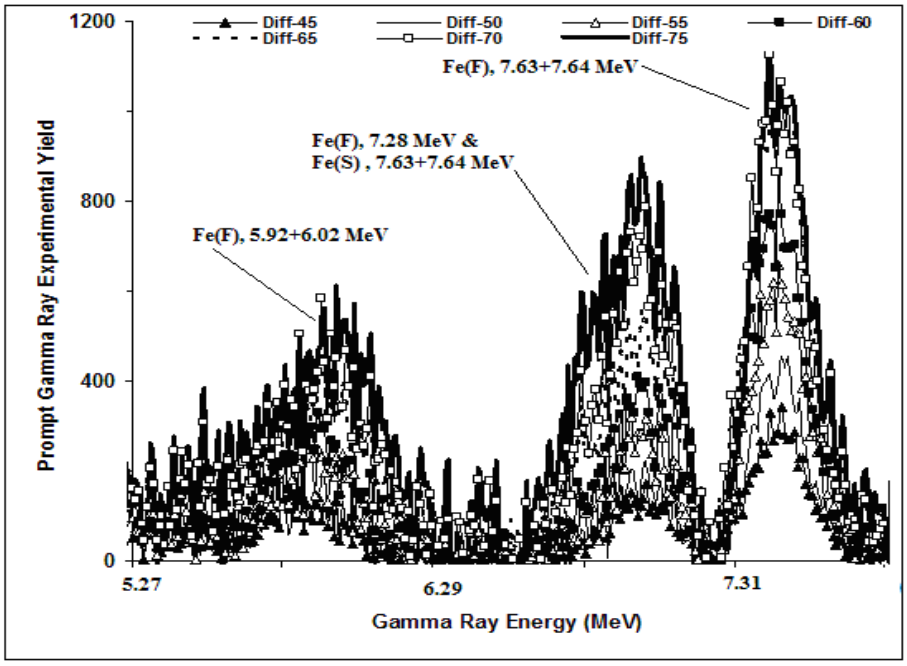

Figure 4.7 Enlarged iron prompt gamma pulse height difference spectra for 45, 50, 55, 60, 65, 70 and 75 keV deuteron beam at 70 μA beam current generated after background subtraction.

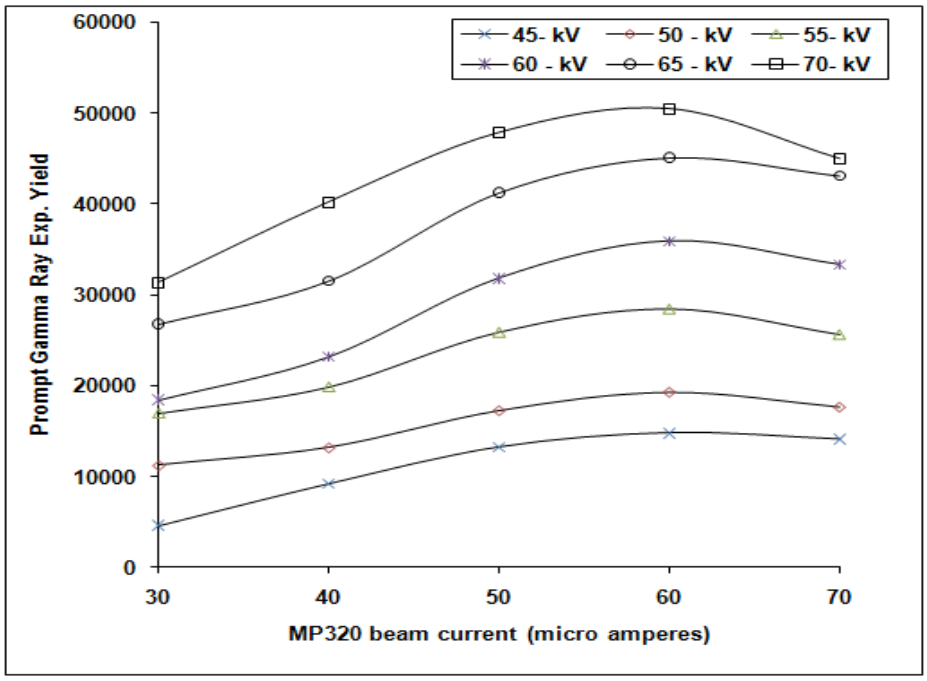

Figure 4.8 Experimental integrated yield of 7.6 MeV prompt gamma rays from iron plotted as a function of 30, 40, 50, 60 and 70 μA beam currents for 45, 50, 55, 60, 65, 70 and 75 keV deuteron beam energies. Line are drawn through the points to show the data trend.

4.2.2 Measure of Chlorine Concentration in Saline Water Samples to test MP320 Based PGNAA Setup Neutron Flux Efficacy

The efficacy of neutron flux from the MP320 generator for its application in prompt gamma analysis of bulk samples was tested through salinity measurement in water samples using the PGNAA setup. The saline water samples were prepared by mixing sodium chloride salt with water in 0.1 to 4.0 wt % of chlorine. The sodium chloride salt was thoroughly mixed with pure water and thereafter poured in cylindrical plastic bottles with 145 mm length and 90 mm internal diameter. Seven saline water specimens were prepared with 1.9, 1.5, 2.0, 2.5, 3.0, 3.5 and 4.0 wt % chlorine. The saline water sample were irradiated in the MP320 based PGNAA setup. The pulsed deuteron beam with 70 keV energy and 70 μA beam current had a pulse width of 5 ns and a frequency of 250 Hz.

Pulsed neutron beam improves signal to background ratio in the PGNAA studies. A BGO detector was used. The prompt gamma-ray data were acquired for a preset time of 25 minutes. As shown in Table 4.2 [33], there are several prompt gamma-ray emitted by chlorine due to capture of thermal neutron. Some of them have energies, which cannot be resolved by BGO detector with 11% energy resolution. The unresolved pair of gamma rays have energies: 1.951 and 1.959; 2.863 and 3.062; 6.619 and 6.627. In this study chlorine prompt gamma-rays with 3.06 (2.863 and 3.062), 4.98, 5.72, 6.11 and 6.63 (6.619 and 6.627) MeV energies were analyzed. Figure 4.9 shows prompt gamma experimental pulse height spectra from chloride contaminated water samples showing prompt gamma rays peaks at 2.86+3.06, 4.98, 5.72, 6.11 and 6.62+6.63.

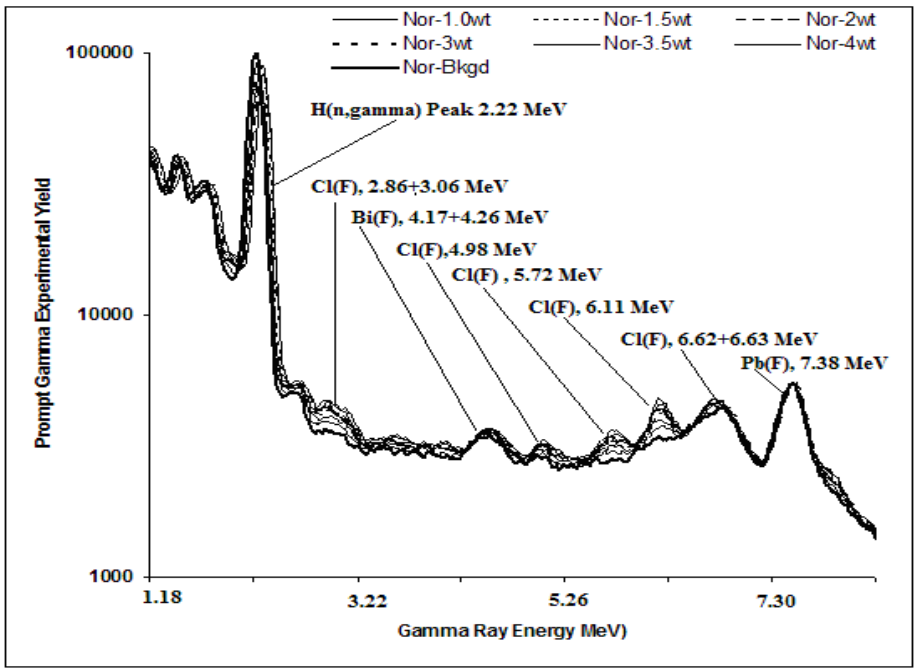

Figure 4.9 Prompt gamma rays experimental pulse height spectrum from chlorinated water samples showing different peaks of prompt gamma rays produced due to capture of thermal neutrons in the chlorine sample.

Figure 4.10 shows enlarged prompt gamma pulse height spectra in excess of 2.81 MeV energies from chloride contaminated water sample containing 1.0, 1.5, 2.0, 3.0, 3.5, and 4.0 wt % chlorine. Also superimposed on the spectra is background gamma ray spectrum. Increasing peak intensity of chlorine prompt gamma rays with increasing chlorine concentration is clearly exhibited in the pulse height spectra of the water samples shown in Figure 4.10. In order to extract the prompt gamma ray yield as a function of chlorine concentration, difference spectra were generated after subtracting background spectrum from pulse height spectra of chloride contaminated water samples. Figure 4.11 shows difference pulse height spectra of prompt gamma rays from chloride contaminated water samples containing 1.0, 1.5, 2.0, 3.0, 3.5, and 4.0 wt %. The chlorine prompt gamma ray peaks corresponding to 3.06 (2.86+3.06), 4.98, 5.72, 6.11 and 6.67(6.62+6.63) MeV energies are quiet prominently in Figure 4.12. Finally, counts under each peak were integrated to obtain gamma ray integrated yield. The gamma ray yield was further normalized to measurement time. Experimental normalized yield of 3.06, 5.72, 6.11 and 6.67 MeV prompt gamma rays from chlorine is plotted in Figure 4.14 as a function of chlorine concentration. An excellent agreement has been achieved between the experimental data and results of the Monte Carlo simulations (shown with continuous line).

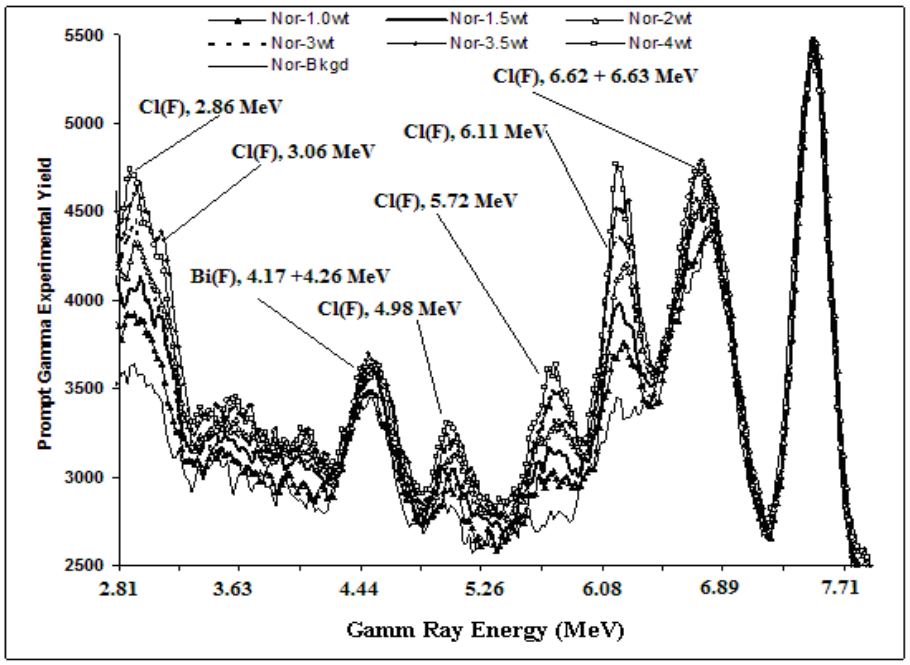

Figure 4.10 Enlarged prompt gamma rays experimental pulse height spectra above 2.8 MeV gamma-ray energy from chlorinated water sample

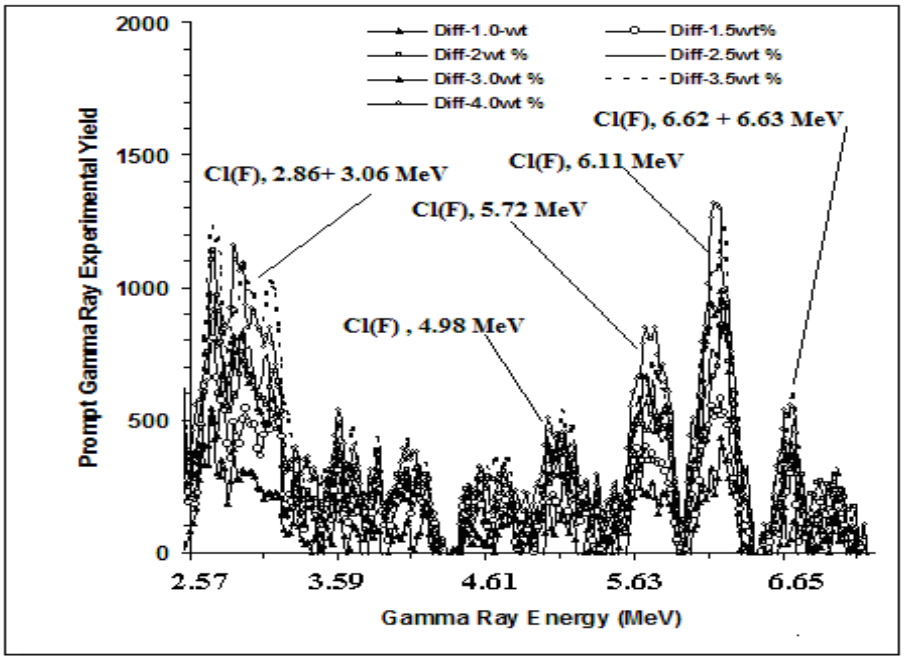

Figure 4.11 Enlarged prompt gamma rays difference pulse height spectra from chlorinated water samples

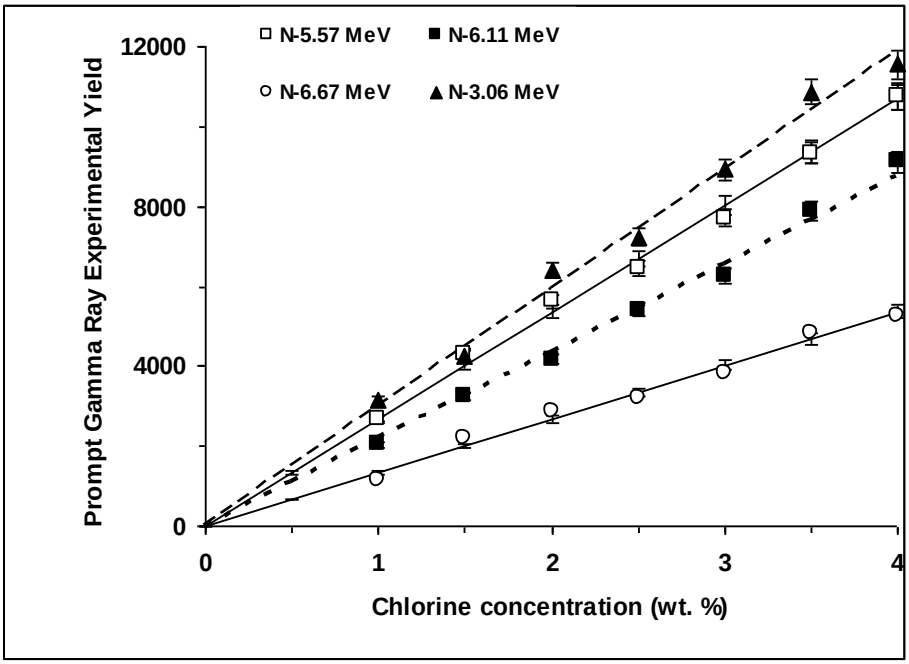

Figure 4.12 Experimental integrated yields of 3.06, 5.72, 6.11 and 6.67 MeV prompt gamma rays from chlorine potted as a function of chlorine concentration. Line represents the results of the Monte Carlo simulations.

CHAPTER FIVE

PROMPT GAMMA-RAYS RESPONSE OF LANTHANUM-HALIDE DETECTORS

In this chapter, the results of lanthanide-halides ($LaBr_3$:Ce and $LaCl_3$:Ce) detectors based PGNAA setup will be discussed for detection of low energy prompt gamma of boron in boron contaminated water samples. Prompt gamma studies were carried out to measure prompt gamma ray yield from boron bulk samples with different concentrations using lanthanide-halide detectors. The same experimental setup discussed in details in chapter 4, was used. The 3 inches x 3 inches $LaBr_3$:Ce and $LaCl_3$:Ce detectors were coupled to a fast photomultiplier with 3 inches diameter. Also detectors have a build in integrated preamplifier to process a signal [42, 44].

5.1 Boron-Contaminated Water samples

Boron was thoroughly mixed with pure water and thereafter poured in cylindrical plastic bottles with 14 cm length and 9 cm internal diameter. Samples were prepared by mixed 0.500, 0.250, 0.125, 0.03125 and 0 (water only) weight % of boron with a known volume of water [42, 44].

5.2 Dead Time Correction (DTC)

Detectors signals were acquired using standard NIM electronics modules. For each detector, the signal, that was routed through a preamplifier, was processed through a spectroscopy amplifier with shaping time of 1 μs. Logical gate signal was generated for each signal processed by the amplifier using single channel analyzer and gate and delay generators modules. For dead time correction, one of the outputs of the gate and delay generator was used to gate Multichannel Buffer, while another output was used to calculate dead time correction.

Dead time correction (DTC) was calculated at the end of each experimental run from the integrated count in the stored spectrum N_{tot} and total gate signals N_{gates}, counted independently through the relation [42, 44, 47]:

$$DTC = [(N_{gates} - N_{tot}) / N_{gates}]. \quad (5.1)$$

Then, dead time corrected experimental yield of counts under a peak $Y_{DTC\text{-}Corr}$ were obtained from experimental counts under the peak Y_{exp} using the relation:

$$Y_{DTC\text{-}Corr} = Y_{exp} [1 + DTC] \quad (5.2)$$

5.3 Prompt Gamma-Ray Yield Measurement Using $LaBr_3$:Ce Detector

Boron concentration in water samples were measured using the KFUPM portable neutron generator model MP320 based PGNAA setup. Four boron samples with 0.03125, 0.125, 0.250 and 0.5 wt. % boron concentration were prepared. The water samples were then irradiated in the newly designed MP320 generator based PGNAA setup. The prompt gamma rays produced from B specimens were detected by 3 inches by 3 inches (diameter x length) $LaBr_3$:Ce detector. For each run the data was taken for 25 minutes [42].

5.3.1 Measurement of $LaBr_3$:Ce detector activation spectrum

In the PGNAA studies, during the irradiation of the samples, the $LaBr_3$:Ce detector, although shielded, is also exposed to thermal neutrons and it registers the prompt gamma-rays due to capture of thermal neutrons in La, Br and Ce elements present in $LaBr_3$:Ce detector. This activation spectrum of the detector also contains additional peaks due to intrinsic activity of the detector. Energies and intensities of prominent prompt gamma-rays due to capture of thermal neutrons in lanthanum, cerium and barium are listed in Table 5.1 [48]. Also, energies of gamma-rays due to intrinsic activity of the detector. All these peaks are present in the sample spectra taken with the detector and needed to be subtracted as beam associated background.

Figure 5.1 shows the intrinsic activity pulse height spectrum of the $LaBr_3$:Ce detector taken with a ^{137}Cs source. This figure also shows Cs peak along with intrinsic activity lines due to ^{138}La isotope. The detector has 3.3% energy resolution for 662 keV gamma-rays from ^{137}Cs. Three intrinsically produced photon peaks from the decay of La are generally observed at 32 keV, 789 keV and 1436 keV [6]. The 32 keV X-ray peak is produced by 32.2 keV K shell X-ray fluorescence of Br; where Br is produced due to the electron capture of La. The 789 keV and 1436 keV gamma lines originate from the beta decay and electron capture branches, respectively, of La [6]. In Figure 5.1, only 789 keV gamma line (sitting on the beta continuum) and 1468 keV gamma-ray peak (sum line of 32 keV X-ray fluorescence peak and 1436 keV gamma line) are shown. The abnormal width of the sum line of 32 keV X-ray fluorescence peak and 1436 keV gamma line may be due to overlapping of 1436 keV gamma line from La with 1460 keV line of ^{40}K, originating from the glass of the photomultiplier tube [6, 42]. The detector was exposed to

fast as well as thermal neutron flux in the portable neutron generator based PGNAA setup and prompt gamma-ray yield spectrum was recorded from the detector without sample. A pulsed beam of 2.5 MeV neutrons was produced via D(d,n) reaction using 70 mA beam of 70 keV deuteron. The deuteron pulse had a width of 5 ns and a frequency of 250 Hz. Figure 5.2 shows beam associated background spectrum of the $LaBr_3$:Ce detector taken during 20 min of run. Due to short irradiation time delayed gamma-rays from ^{140}La (half life=40.3 h) could not be detected. Figure 5.2 shows the intrinsic activity line along with prompt gamma-ray due to activation of La, Br and Ce elements in the detector. Also shown in the spectrum is 2.22 MeV hydrogen capture peak in the moderator and neutron shielding of the detector. Aluminum (Al) prompt gamma peak presents because of aluminum material using in the detector. Most of the prompt gamma-ray lines of lanthanum, cerium and bromine listed in Table 5.1 have been identified in Figure 5.2.

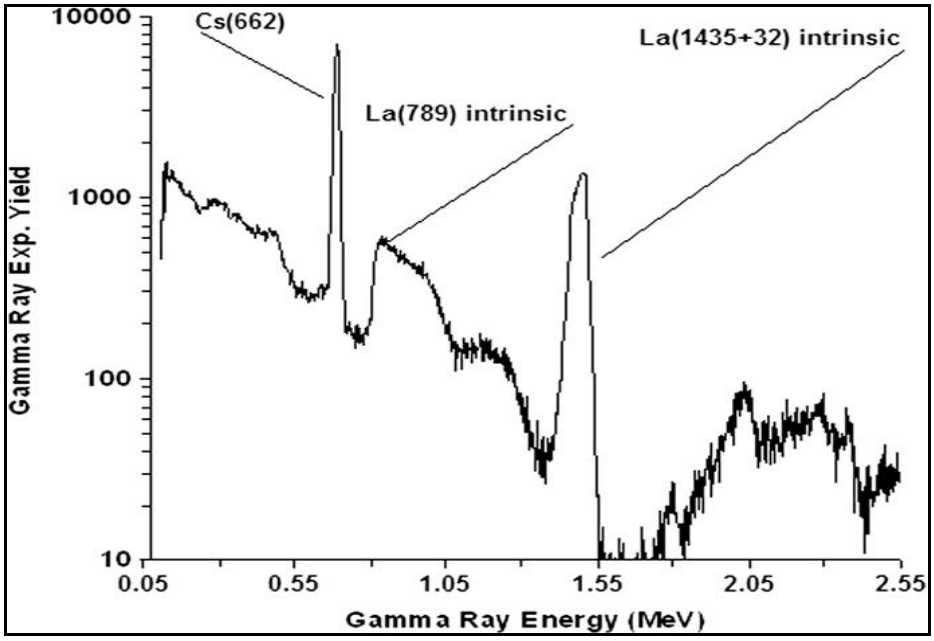

Figure 5.1 $LaBr_3$:Ce pulse height spectrum taken with ^{137}Cs source exhibiting ^{137}Cs peak along with detector intrinsic activity peaks due to La.

TABLE 5.1 Energies and Partial Elemental Cross Section $\sigma_\gamma^Z(E_\gamma)$-barns of Prominent Capture Gamma-Rays of Boron, Bromine, Cerium and Lanthanum [42, 44, 48].

Element	**Gamma-Ray Energy (keV)**	**$\sigma_\gamma^Z(E_\gamma)$-barns**
B(n,α)	478	716
Br	196	0.434
	271	0.462
	275	0.158
	315	0.460
	367	0.223
	513	0.210
	661	0.082
	828	0.285
	1248	0.0527
Ce	475	0.082
	1107	0.040
La	163	0.489
	272	0.502
	288	0.730
	567	0.335
	595	0.103
	789	intrinsic
	1436	intrinsic

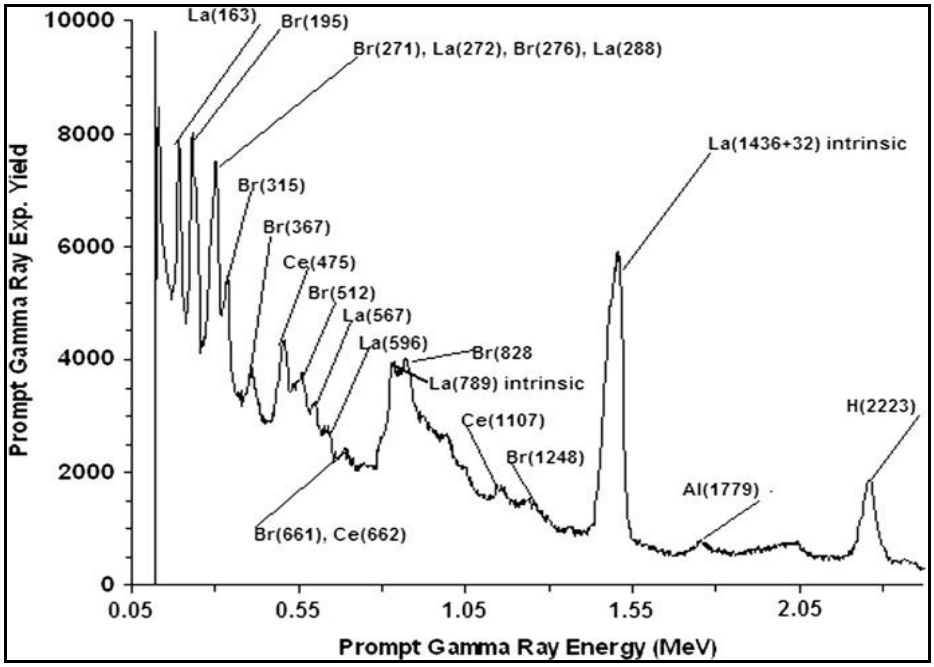

Figure 5.2 Prompt gamma-ray spectrum due to activation of the LaBr:Ce detector caused by capture of thermal neutrons in La, Br and Ce elements present in LaBr:Ce detector

5.3.2 Prompt Gamma-Ray Analysis of Boron-Contaminated Water Samples

Dead time was calculated for prompt gamma-ray spectra of boron water samples using Eqs. (5.1) and (5.2). As expected dead time was smaller for lower concentration samples and increased with increasing concentration. For four boron samples with 0.031, 0.125, 0.250 and 0.50 wt % boron, the dead time correction was calculated to be: 3.8, 5.0, 8.8 and 25 %, respectively [42]. For each boron run the data were acquired for 25 min. Figure 5.3 shows the prompt γ-rays spectrum of water sample contains 0.5 wt. % of boron. The main feature of Figure 5.3 is the presence of the 478 (keV) boron prompt gamma ray peak along with capture gamma ray peak from hydrogen present in the water and moderator. This peak can be used to extract the boron concentration information. Figure 5.4 shows pulse height spectra of prompt gamma-rays from water samples containing 0.031, 0.125, 0.250 and 0.5 wt. % boron superimposed upon each other along with background

spectrum taken with pure water sample. In order to show effect of increasing concentration of boron on the pulse height spectrum, pulse height spectra for different boron concentration are plotted with a constant vertical offset. The 478 keV boron gamma-ray peak along with intrinsic 1436 keV intrinsic activity peak and 2223 keV hydrogen capture peak from moderator are quite prominent. Figure 5.5 shows 478 keV boron peak on enlarged scale to show its interference with the 475 keV peak from activation of cerium in LaBr3 detector. Since boron peaks contain the contribution of Ce (475) peak, difference spectra of boron peaks for 0.031, 0.125, 0.250 and 0.500 wt% concentration were generated by subtracting the background spectrum from each of them. Figure 5.6 shows gamma ray spectra for 478 keV boron peaks after background subtraction. The enhanced increase in intensity of 478 keV boron prompt gamma rays with increasing boron concentration is quiet prominent. Finally, gamma-ray yield was integrated under the boron peaks and was plotted as a function of boron concentration. The integrated boron yield data was corrected for dead time using equations (5.1) and (5.2). Figure 5.7 shows dead time corrected and background subtracted counts of four boron samples as a function of boron concentration for boron contaminated water samples. Within the experimental uncertainties, there is a linear correlation between the 478 keV prompt gamma ray yield and boron concentrations. The solid line in Figure 5.7 represents the results of calculated yield of prompt gamma-ray obtained from Monte Carlo calculation following the procedure described in chapter 3. There is an excellent agreement between the theoretical yield and experimental yield of prompt gamma-ray from boron measured by LaBr detector as a function of B concentration in water samples [42].

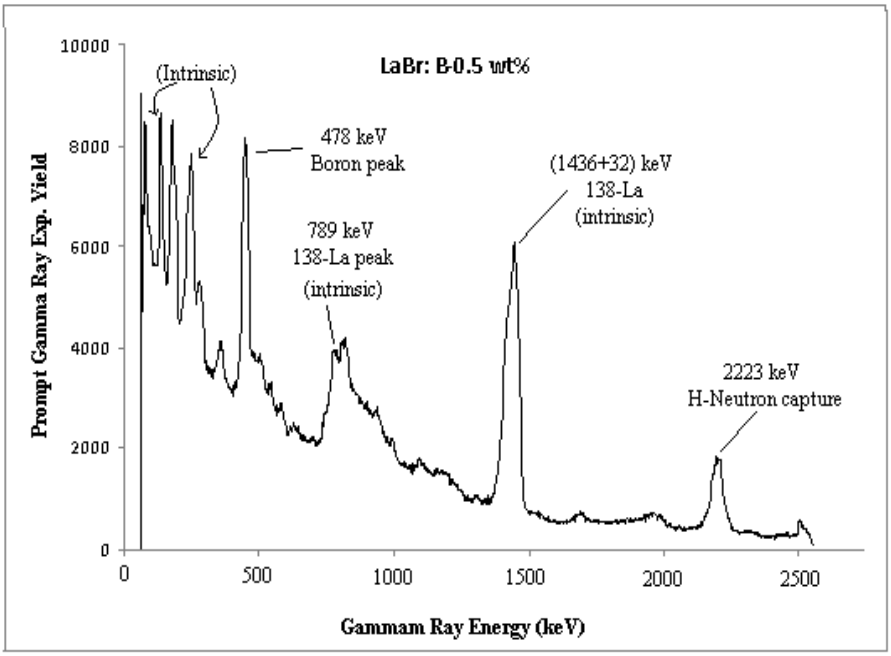

Figure 5.3 prompt γ-rays spectrum of water sample contains 0.5 wt. % boron obtained with LaBr detector

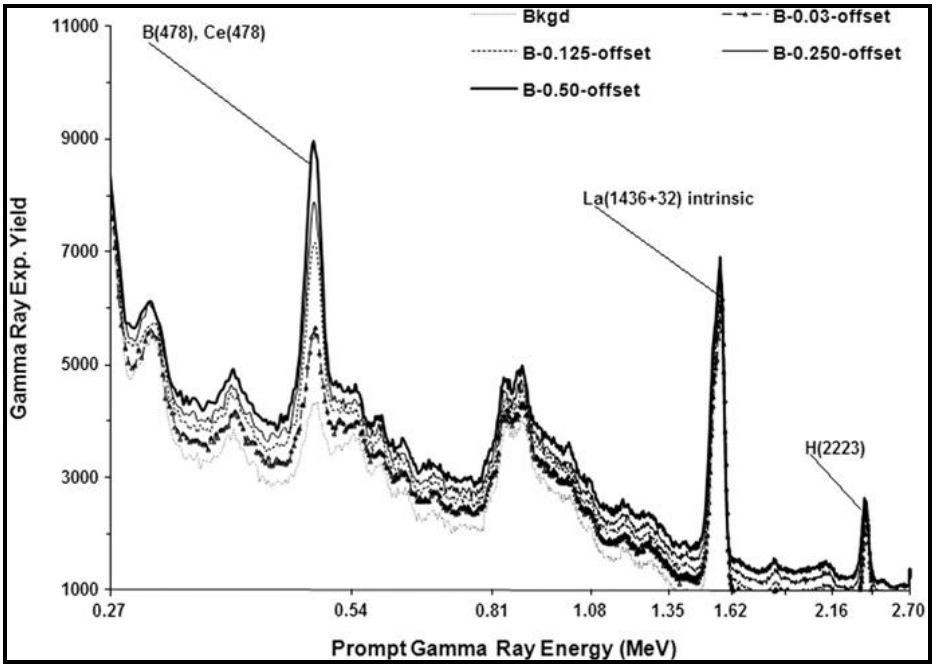

Figure 5.4 Prompt gamma-rays pulse height spectra of four boron contaminated water samples obtained by LaBr detector.

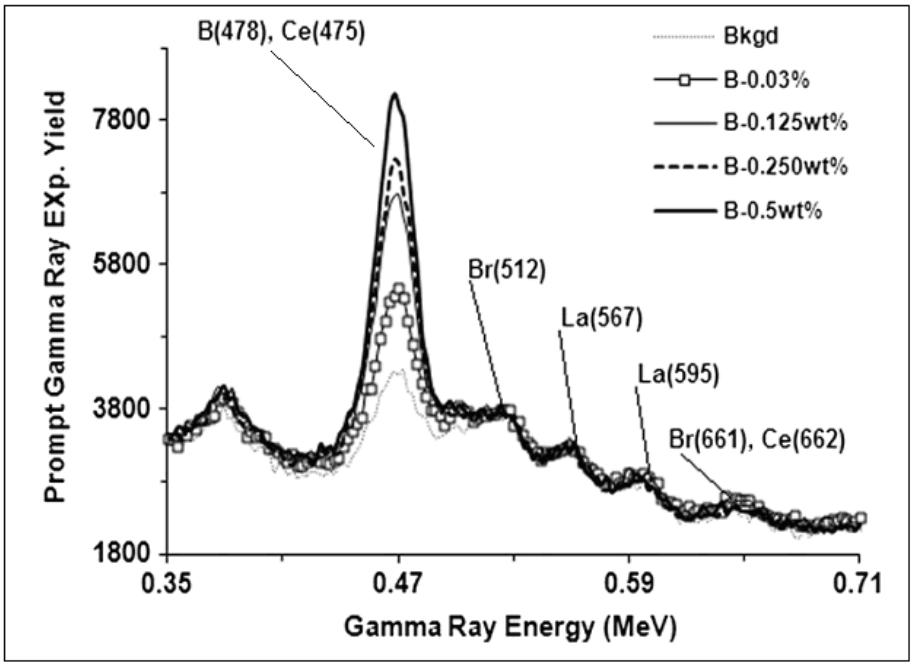

Fig. 5.5 The enlarged spectrum of boron peak gamma ray superimposed upon each other for pure water and water containing 0.5, 0.25, 0.125 and 0.03125 wt.% of boron, obtained with LaBr detector

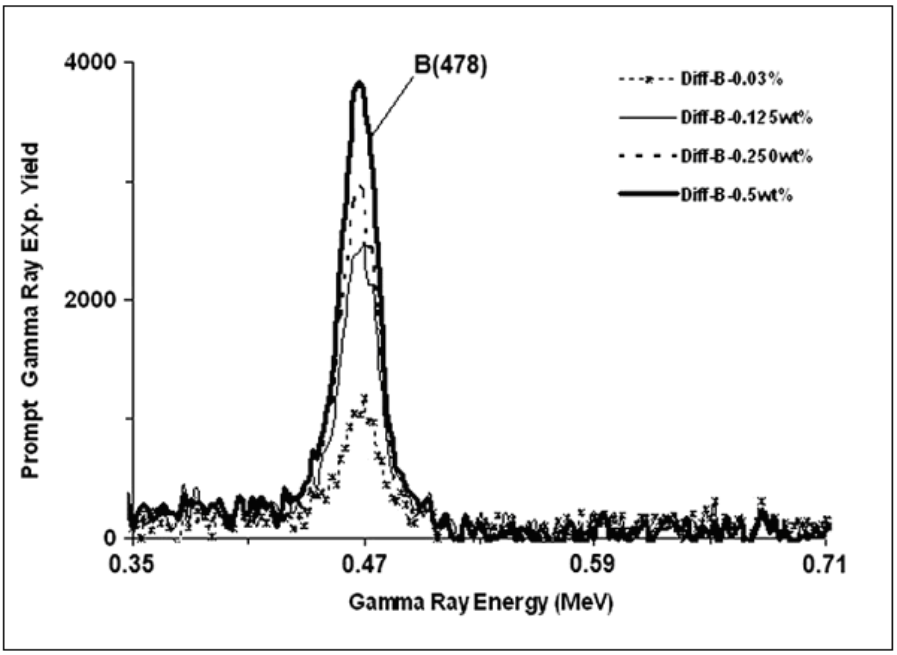

Fig. 5.6 prompt gamma ray spectra for boron samples after background subtraction obtained with LaBr detector

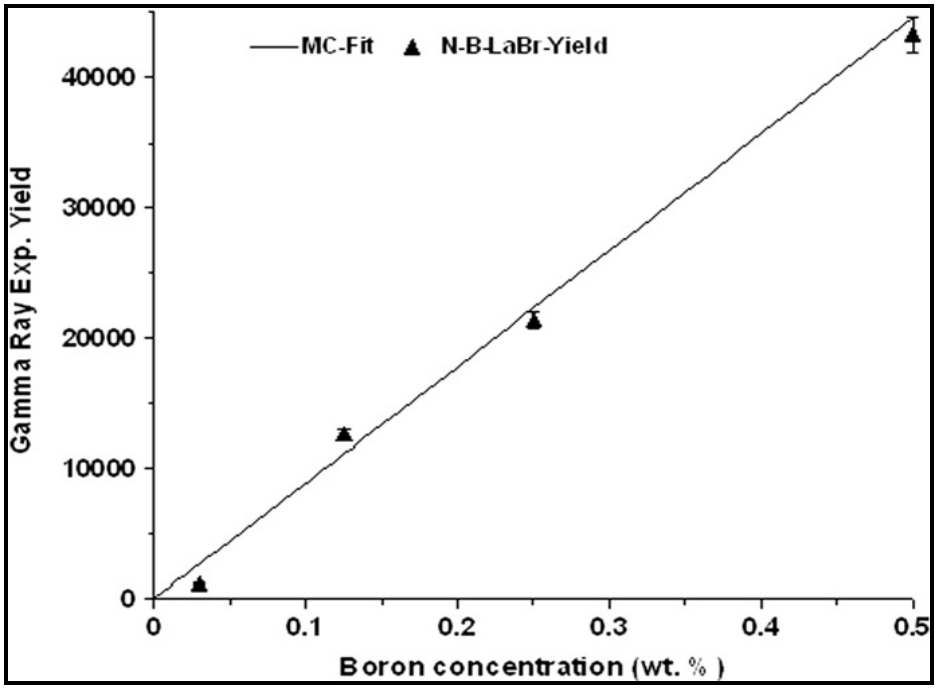

Figure 5.7 Integrated dead time corrected yield of 478 keV prompt gamma-ray of boron from four water samples plotted as a function of boron concentration. The solid line shows normalized-calculated yield of the gamma-rays obtained through Monte Carlo calculations [42].

5.3.3 Minimum Detection Concentration (MDC) of Boron in Water Samples

The MDC measured under a peak with net counts N_P and associated background counts N_B (under the peak) is defined by the relation [49]:

$$MDC = 4.653 * (C/ N_P) * \sqrt{N_B}\,; \quad (5.3)$$

where C is the element's concentration in the peak. The error in MDC is given by:

$$\sigma_{MDC} = (C/ N_P)*[\sqrt{(2*N_B)}] \quad (5.4)$$

The minimum detection concentration (MDC) of KFUPM portable neutron generator based PGNAA of boron in water samples, using $LaBr_3$:Ce detector was calculated using equations (5.3) and (5.4). The minimum detection concentration MDC of boron and its standard deviation σ_{MDC} was calculated to be: MDC = 30.1 ppm and σ_{MDC} = 9.3 ppm [42].

5.4 Prompt Gamma-Ray Yield Measurement Using $LaCl_3$:Ce Detector

Boron concentration in water samples were measured using the KFUPM portable neutron generator model MP320 based PGNAA setup. The prompt gamma rays produced from the B specimens were detected by 3 inches by 3 inches (diameter x length) $LaCl_3$:Ce detector. For each run the data was taken for 25 minutes [44].

5.4.1 Intrinsic Activity and Beam Associated Background Spectra of $LaCl_3$:Ce Detector

During the irradiation of the water samples, the detector, although shielded was also exposed to thermal neutrons and it registered the prompt gamma rays due to capture of thermal neutrons in La, Cl and Ce elements present in $LaCl_3$:Ce detector. These peaks were present in the boron containing water spectra and needed to be subtracted as beam associated background [75]. Energies and intensities of prominent prompt gamma-rays due to capture of thermal neutrons in lanthanum, cerium and chlorine are listed in Table 5.1 and Table 5.2 [44, 48]. All these peaks are present in the sample spectra taken with the detector and needed to be subtracted as beam associated background. In the present study, intrinsic activity and beam associated background spectra of $LaCl_3$:Ce detector were studied in detail. The detector signal was acquired using standard NIM electronics modules [44]. Figure 5.8 shows the intrinsic activity pulse height spectrum of the $LaCl_3$:Ce detector taken with a ^{137}Cs source. In order to show the location of intrinsic activity in the activation spectrum of the detector, activation spectrum is superimposed upon intrinsic activity spectrum of the detector. This figure also shows Cs peak along with intrinsic activity lines due to ^{138}La isotope. The detector has 4 % energy resolution

for 662 keV gamma-rays from ^{137}Cs. The pulse height spectrum of the $LaCl_3$:Ce detector taken with a ^{137}Cs, is nearly like the spectra taken with $LaBr_3$:Ce detector, because the deference between the two detectors are Br and Cl elements, where both Br and Cl are not radio active isotopes. Three intrinsically produced photon peaks from the decay of ^{138}La are generally observed at 32 keV, 789 keV and 1436 keV, as shown in Figure 5.8, with 662 keV ^{137}Cs peak. In order to record activation spectrum of the $LaCl_3$:Ce detector, it was irradiated with fast as well as thermal neutron flux in the portable neutron generator based PGNAA set up and prompt gamma-ray yield spectrum was recorded from the detector without sample. A pulsed beam of 2.5 MeV neutrons was produced via D(d,n) reaction using 70 μA beam of 70 keV deuteron. The deuteron pulse had a width of 5 ns and a frequency of 250 Hz [44]. Figure 5.9 shows beam associated background spectrum of the LaCl detector taken during 20 minutes of run. Due to short irradiation time delayed gamma-rays from ^{140}La (half life = 40.3 h) could not be detected. Figure 5.9 shows the intrinsic activity line along with prompt gamma-ray due to activation of La, Cl and Ce element in the detector. Also shown in the spectrum is 2.22 MeV hydrogen capture peak in the moderator and neutron shielding of the detector. Most of the prompt gamma-ray lines of lanthanum, cerium and chlorine with energies below 2.22 MeV, listed in Table 5.1 and Table 5.2, have been identified in Figure 5.9.

TABLE 5.2 Energies and Partial Elemental Cross Section $\sigma_\gamma^z(E_\gamma)$-barns of Prominent Capture Gamma-Rays of Chlorine [44, 48].

Element	**Gamma-Ray Energy (keV)**	**$\sigma_\gamma^z(E_\gamma)$-barns**
Cl	517	7.58
	786	3.420
	788	5.42
	1165	8.91
	1601	1.21
	1951	6.33
	1959	4.10

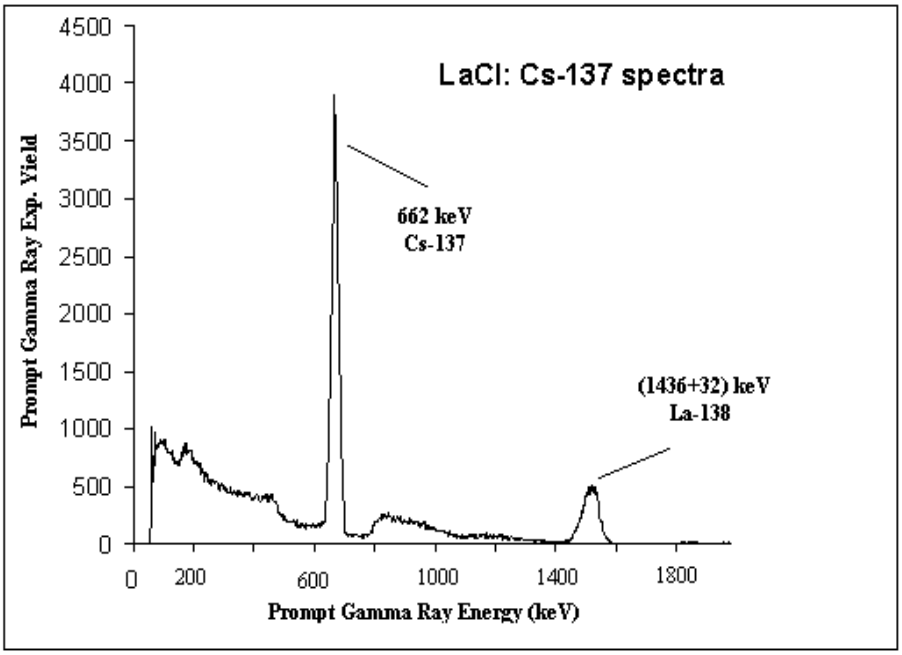

Figure 5.8 Pulse height spectrum of the $LaCl_3$:Ce detector taken with a ^{137}Cs source

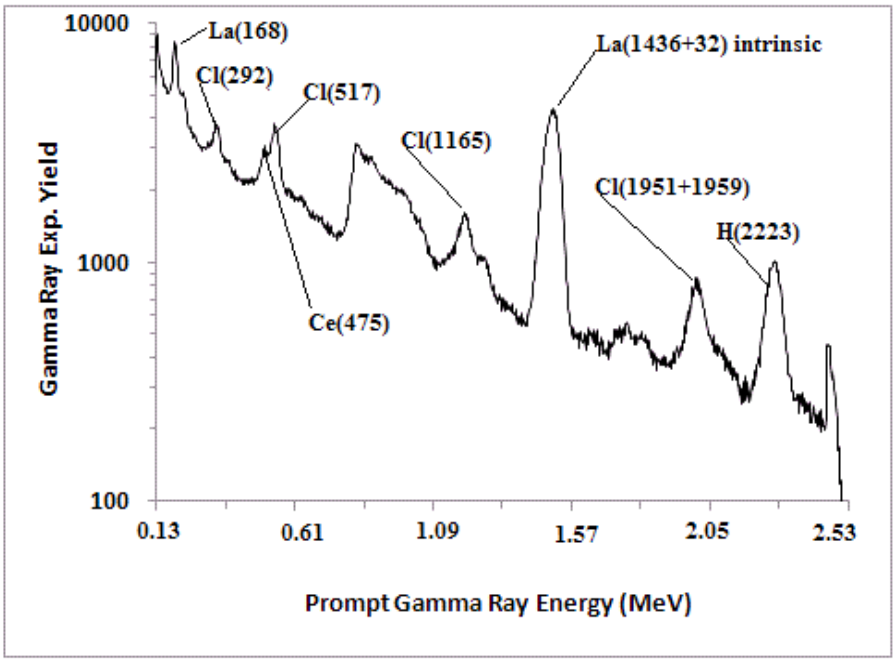

Figure 5.9 Prompt gamma-ray spectrum due to activation of the LaBr:Ce detector caused by capture of thermal neutrons in La, Cl and Ce elements present in LaCl:Ce detector.

5.4.2 Prompt Gamma-Ray Analysis of Boron-Contaminated Water Samples

Dead time was calculated for prompt gamma-ray spectra of boron water samples using Eqs. (5.1) and (5.2). For four boron samples with 0.031, 0.125, 0.250 and 0.50 wt % boron, the dead time correction was calculated to be: 0.15, 0.20, 0.35 and 1.0 %/min, respectively [44]. For each boron run the data were acquired for 25 min. Fig. 5.10 shows a prompt g-rays spectrum of a water sample containing 0.5 wt% boron concentration. In addition to prompt gamma-ray peaks for La, Cl, Ce and Al present in the beam associated background spectrum, new peak from boron was observed at 478 keV. The 478 keV peak had interference with 475 cesium (Ce) peak. Figure 5.11 shows pulse height spectra of prompt gamma-rays from water samples containing 0.031, 0.125, 0.250 and 0.5 wt. % boron superimposed upon each other along with background spectrum taken with pure water sample. In order to show effect of increasing concentration of boron on the pulse

height spectrum, pulse height spectra for different boron concentration are plotted with a constant vertical offset. Fig. 5.12 shows the enlarged view of the superimposed spectra of 478 keV prompt gamma-rays spectra for five boron-contaminated water samples. As shown in 5.12, the background under 478 keV boron peak can be subtracted easily using pure water spectrum as a background spectrum. Figure 5.13 shows 478 keV B prompt gamma ray peak after background subtraction. The intensity of the 478 keV peak increases gradually with the boron concentration. The Dead time corrected integrated yield of the 478 keV peak after background subtraction is plotted as a function of boron concentration in water over 0.03125–0.500 wt% boron concentration, as it is shown in Figure 5.14. There is a linear correlation between the prompt gamma-ray yield and the boron concentration plotted in Figure 5.14. The solid line in Figure 5.14 represents the results of calculated yield of prompt gamma-ray obtained from Monte Carlo calculation. There is an excellent agreement between the theoretical yield and experimental yield [44].

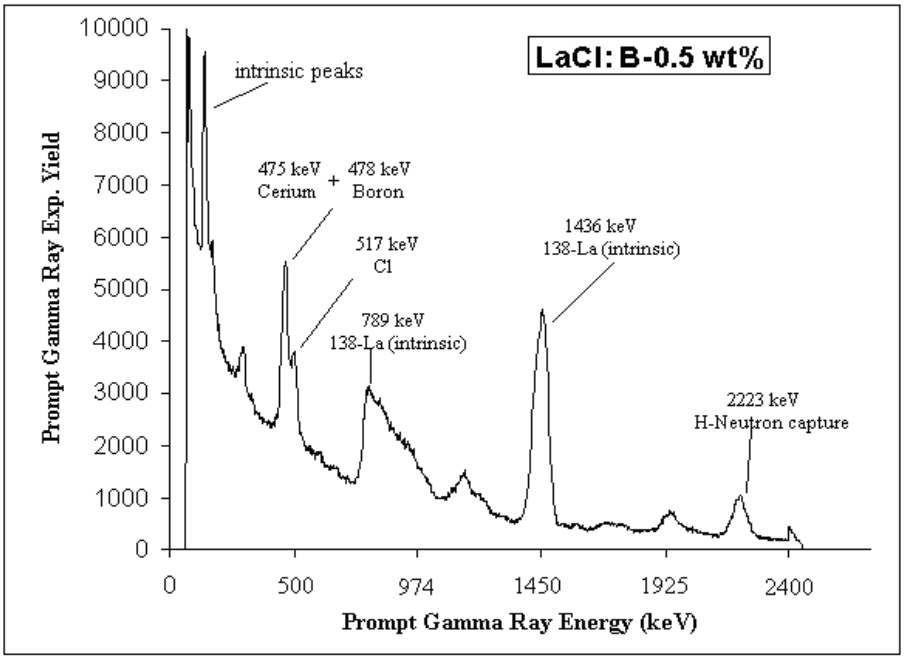

Figure 5.10 prompt γ-rays spectrum of water sample contains 0.5 wt. % boron obtained with LaCl detector

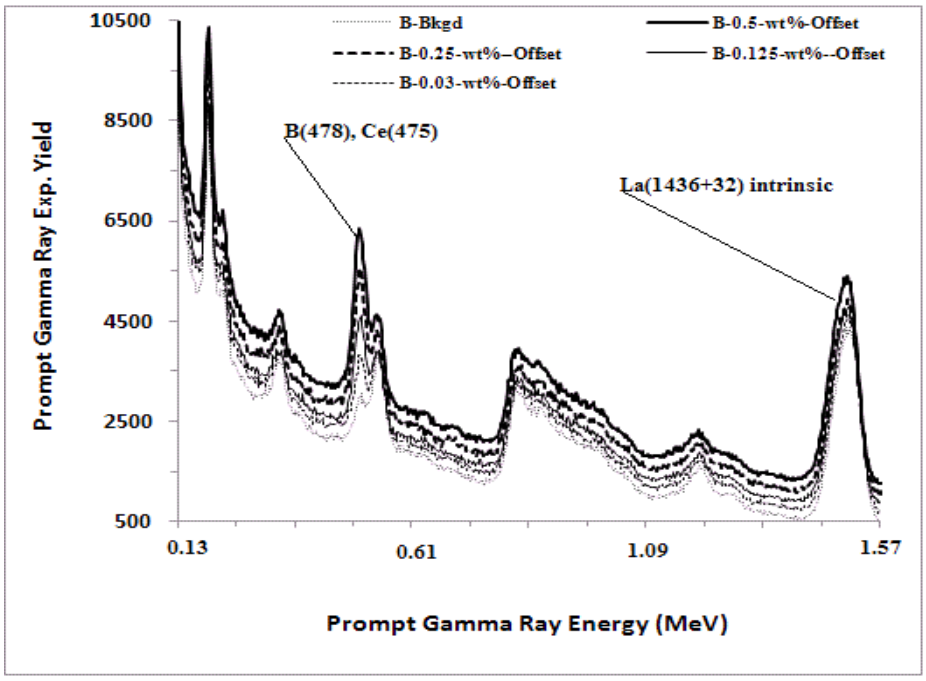

Figure 5.11 Prompt gamma-rays pulse height spectra of four boron contaminated water samples obtained with LaCl detector, plotted with a constant vertical offset.

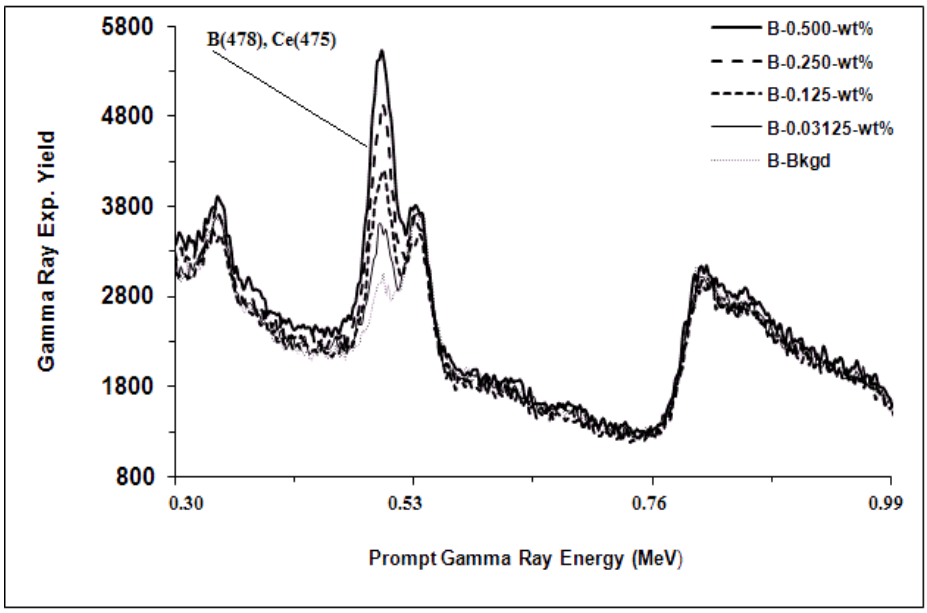

5.12 The enlarged spectrum of boron peak gamma ray superimposed upon each other for pure water and water containing 0.5, 0.25, 0.125 and 0.03125 wt.% of Boron, obtained with LaCl detector, showing the interference of 478 keV boron peak and 475 keV Ce peak.

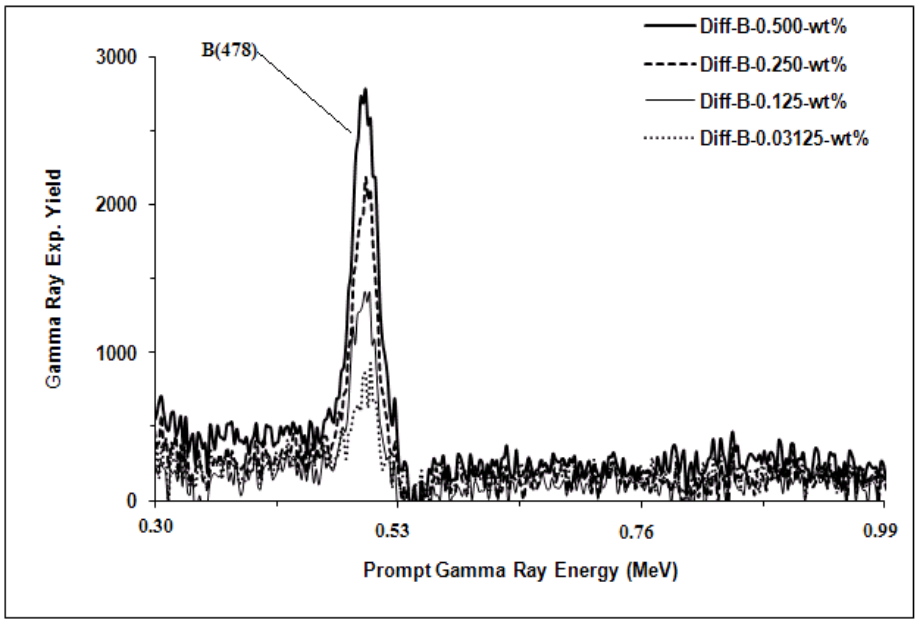

Figure 5.13 Enlarged prompt gamma-ray experimental pulse height spectra after background subtraction from the four boron-contaminated water samples.

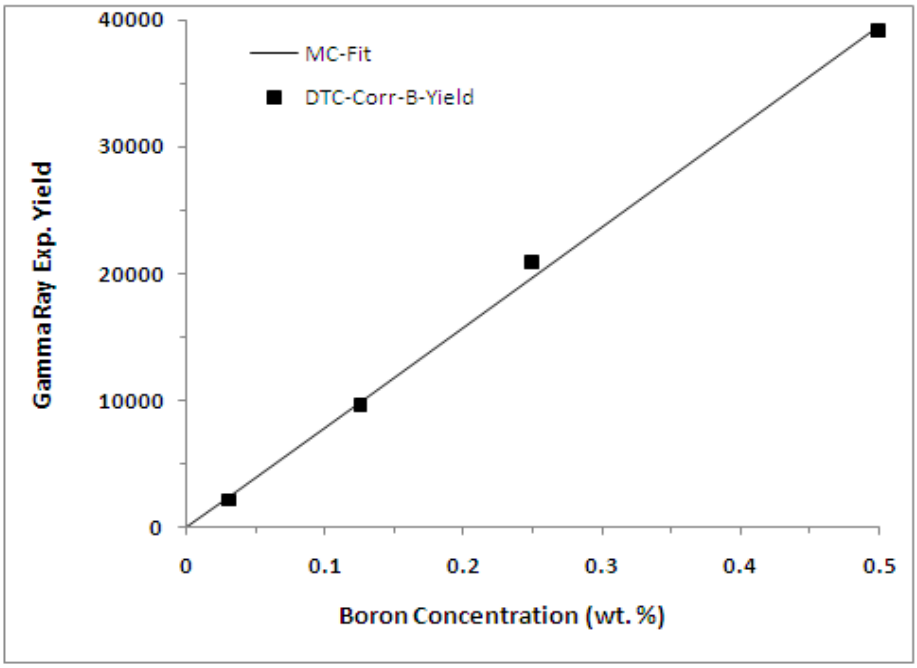

Figure 5.14 Dead time corrected integrated yield of 478 keV prompt gamma-ray of boron from four water samples plotted as a function of boron concentration. The solid line shows normalized-calculated yield of the gamma-rays obtained through Monte Carlo calculations [44].

5.4.3 Minimum Detection Concentration (MDC) of Boron in Water Samples

The minimum detection concentration (MDC) of KFUPM portable neutron generator based PGNAA setup was determined from LaCl:Ce detector using equations (5.3) and (5.4). For 90 mm x 140 mm (diameter x height) cylindrical water sample; minimum detection limit of boron MDC and its standard deviation σ_{MDC} was calculated to be: MDC = 45.0 ppm and σ_{MDC} = 16.4 ppm [44].

CHAPTER SIX

PERFORMANCE TEST OF BISMUTH GERMINATE (BGO) DETECTOR

Tests of a large volume Bismuth Germinate (BGO) detector were carried out to detect low energy prompt gamma-rays from boron-contaminated water samples using a portable neutron generator-based prompt gamma neutron activation analysis (PGNAA) setup. The same experimental setup described in chapter 4 has used. We used the same boron samples discussed in chapter 5 with samples preparation [43].

6.1 Background Spectrums of BGO Detector Description

During the irradiation of the samples, the BGO detector, although well shielded, was also exposed to thermal neutrons and it registered the prompt gamma-rays due to the capture of thermal neutrons in Bi and Ge elements present in the BGO detector. The energies and intensities of prominent prompt gamma-rays due to capture of thermal neutrons in detector material and boron elements are listed in Table 1 [48]. All these peaks are present in Figure 6.1 showing beam associated background spectrum of the BGO detector. In addition, it is shown in Figure 6.1 the 2.223 MeV hydrogen thermal neutron capture peak

in the moderator and neutron shielding of the detector. Most of the prompt gamma-ray lines of Bi and Ge listed in Table 6.1 [48] have been identified in Figure 6.1. Due to the poor energy resolution of the BGO detector (11% for 662 keV gamma-rays from ^{137}Cs source), the detector could not resolve 597 and 608 keV prompt gamma-rays of germanium from that of 674 keV prompt gamma-rays from bismuth [48]. Figure 6.2 shows 500 keV germanium peak after background substation. The FWHM of 500 keV of germanium peak, as shown in Figure 6.2, was measured to be 18.4 $\pm$1.5 % [43].

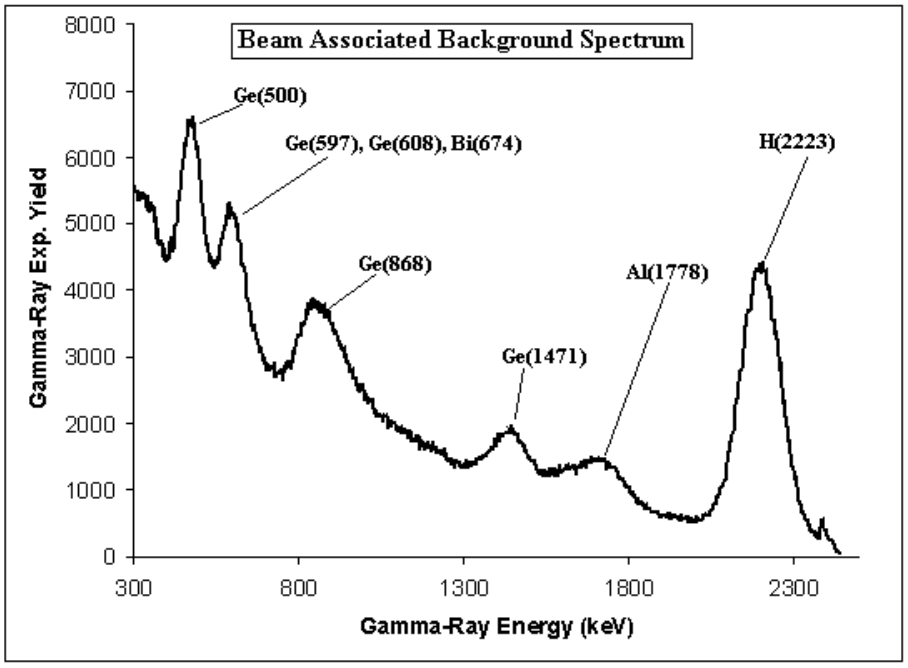

Figure 6.1 Prompt gamma-ray spectrum due to activation of the BGO detector caused by the capture of thermal neutrons in Bi and Ge elements present in BGO detector.

TABLE 6.1 Energies and Partial Elemental Cross Section $\sigma_\gamma^z(E_\gamma)$-barns of Prominent Capture Gamma-Rays of Boron, Bismuth and Germanium [43, 48].

Element	**Gamma-ray energy (keV)**	**$\sigma_\gamma^z(E_\gamma)$-barns**
B(n,α)	478	716
Bi	162	0.008
	320	0.0115
	674	0.0026
	2505	0.0021
	2828	0.00179
	4054	0.0137
	4171	0.0171
Ge	175	0.164
	493	0.133
	500	0.162
	596	1.100
	608	0.250
	868	0.553
	961	0.129
	1101	0.134
	1204	0.141
	1472	0.083

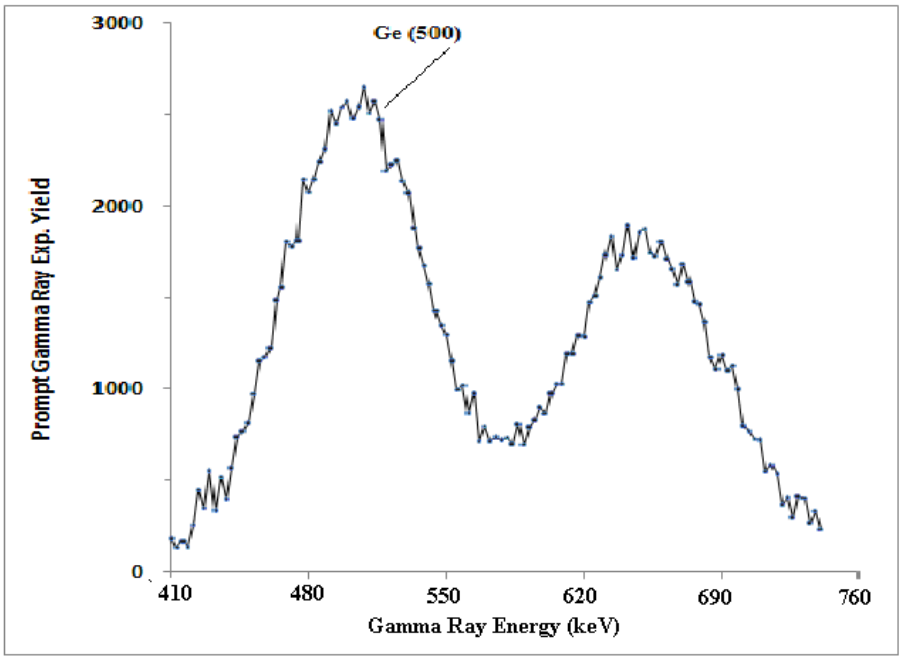

Figure 6.2 Pulse height spectrum of 500 keV prompt gamma-rays of germanium present in the BGO detector after background subtraction.

6.2 Prompt Gamma-Rays Analysis of B-Contaminated Water Samples

Figure 6.3 through Figure 6.6 show the pulse height spectra of BGO detector from boron-contaminated water samples. Figure 6.3 shows the pulse height spectra of prompt gamma-rays from water samples contaminated with 0.031, 0.125, 0.250 and 0.5 wt% boron superimposed upon each other along with the background spectrum taken with the pure water sample. The 478 keV boron gamma-ray peak along with 2223 keV hydrogen capture peak from the moderator is quiet prominent in Figure 6.3. Figure 6.3 also shows the interference of 478 keV boron peak with 500 keV peak from activation of germanium in the BGO detector. Figure 6.4 shows the enlarged spectrum 478 keV boron gamma-ray peaks for the five samples superimposed upon each other [43].

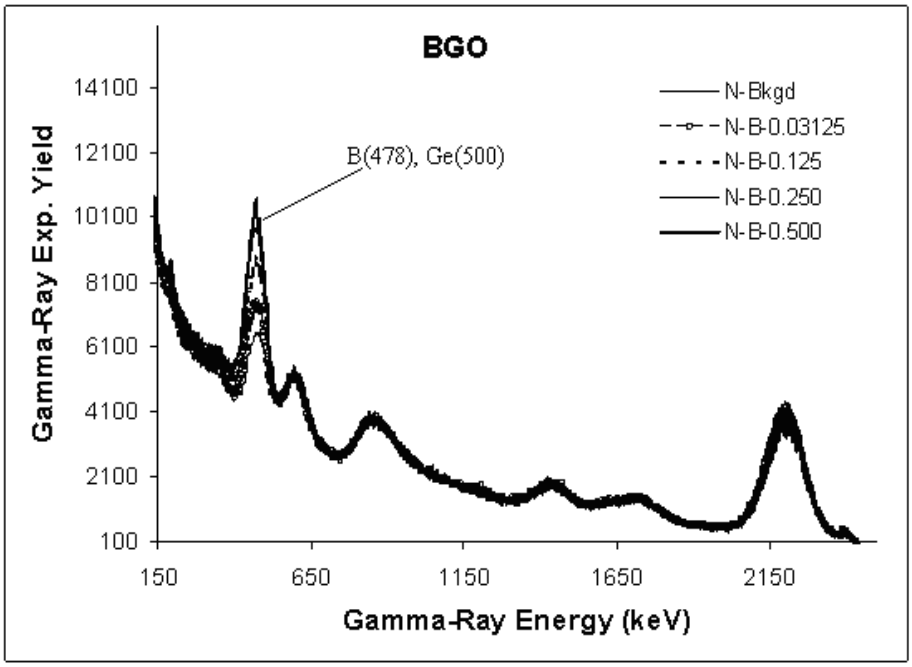

Figure 6.3 Experimental pulse height spectra of boron peak from five boron-water samples superimposed upon each other

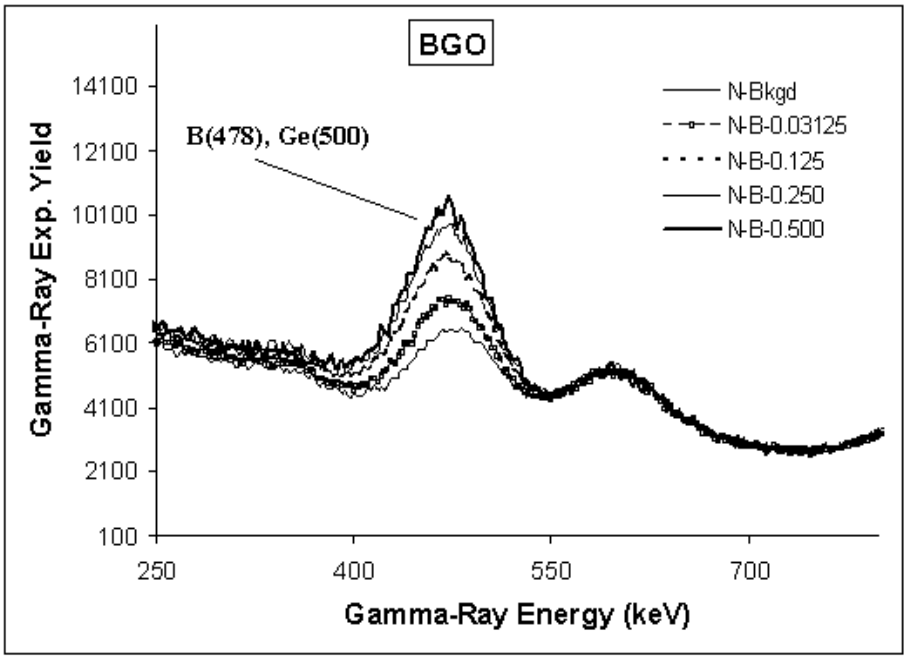

Figure 6.4 The enlarged spectrum of boron peak gamma ray superimposed upon each other for pure water and water containing 0.5, 0.25, 0.125 and 0.03125 wt.% of boron, obtained with LaBr detector,

Since boron peaks contain the contribution of 500 keV peak of germanium, the difference spectra of boron peaks for 0.031, 0.125, 0.250, and 0.500 wt. % boron concentration were generated by subtracting the background spectrum from each of them. Figure 6.5 shows the difference spectra of boron peaks for samples prepared with 0.031, 0.125, 0.250 and 0.500 wt % B concentration. The full width at half maximum (FWHM) of the boron-difference peak was measured to be 16.6±1.5%, which is consistent with the observed value of 18.4±1.5 % FWHM for 500 keV of germanium peak shown in Figure 6.2. In order to study the Doppler broadening of boron-peak, the BGO energy resolution was quite poor and as such it cannot be used to observe the expected broadening of few-tens of keV for the boron peak [43].

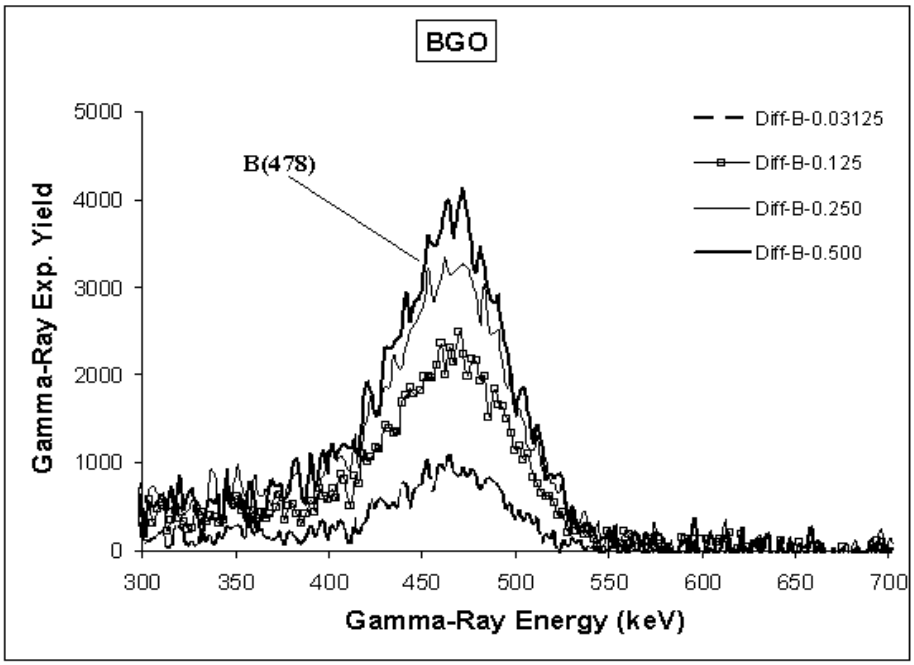

Figure 6.5 Enlarged prompt gamma-ray experimental pulse height spectra after background subtraction from the four boron-contaminated water samples.

Finally, the counts under peaks in the difference spectra were integrated to generate integrated yield as a function of B concentration, as shown in Fig. 6.6. The solid line in Figure 6.6 represents the results of calculated yield of prompt gamma-ray obtained from Monte Carlo calculation following the procedure described in chapter 3. There is an excellent agreement between the theoretical yield and experimental yield of prompt gamma-ray from boron measured by BGO detector as a function of B concentration in the water samples [43].

6.3 Minimum Detection Concentration (MDC) of Boron in Water Samples Using BGO Detector

The minimum detection concentration (MDC) of boron in water samples using BGO detector was calculated using equations (5.3) and (5.4) given in chapter 5. For 90 mm x 140 mm (diameter x height) cylindrical water sample, minimum detection limit of boron MDC = 28 ppm (or 0.0028 wt.%) and its standard deviation σ_{MDC} was calculated to be σ_{MDC}=8 ppm (or 0.0008 wt.%) [43].

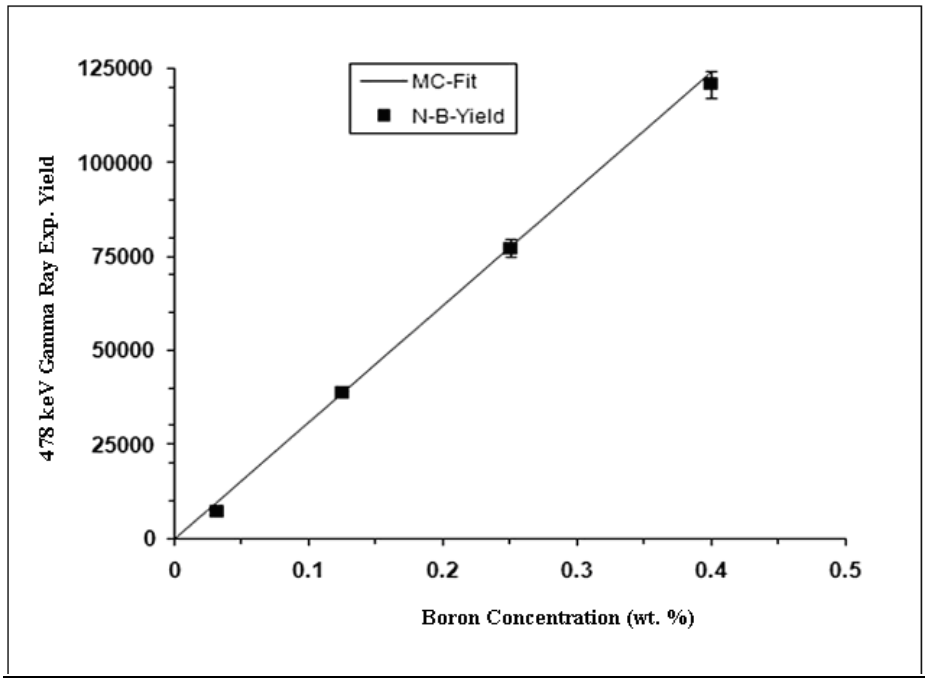

Figure 6.6 Integrated yield of 478 keV prompt gamma-ray of boron from four water samples plotted as a function of boron concentration. The solid line shows normalized-calculated yield of the gamma-rays obtained through Monte Carlo calculations.

CHAPTER SEVEN

INTERCOMPARISON OF MINIMUM DETECTION CONCENTRATION (MDC) FOR LANTHANIDE HALIDES AND BGO DETECTOR

7.1 Minimum Detection Concentration (MDL) for Lanthanide-Halides ($LaBr_3$:Ce and $LaCl_3$:Ce) and BGO Detectors, Inter Comparison

Minimum detection concentrations (MDC)s of KFUPM portable neutron generator based PGNAA setup from LaBr3:Ce, $LaBr_3$:Ce and BGO detectors were determined by using a procedure described in chapter 5. Minimum detection concentrations (MDC)s of boron in water samples for LaBr3:Ce, $LaBr_3$:Ce and BGO detectors are listed in table 7.1.

From Table 7.1 we note that the BGO detector has the lowest MDC, then becomes $LaBr_3$:Ce, and the highest MDC value for $LaCl_3$:Ce detector. The reason behind the lower value MDC for BGO comparing with lanthanum-halide detectors, is the large size of BGO detector. Our BGO detector is 5 x 5 (inches), while the lanthanum-halide ($LaBr_3$:Ce and $LaCl_3$:Ce) detectors have 3 x 3 (inches). So, BGO detector's volume is: 98.175 $(inch)^3$, while lanthanum-halides have: 21.2 $(inch)^3$. Despite the big deference between volumes, lanthanum-halide detectors have comparable MDC values from BGO detector.

We observe from Table 7.1 that $LaBr_3$:Ce has lower MDC value than $LaCl_3$:Ce with 30 ± 9.3 ppm and 45 ±16.4 ppm respectively.

TABLE 7.1 Minimum Detection Concentration (MDC) of the KFUPM PGNAA Setup for Boron in Water Samples for LaBr3:Ce, $LaBr_3$:Ce and BGO Detectors. (MDC) in Parts Per Million (ppm) Unit.

Detector	**MDC (ppm) for Boron in Water Samples**
$LaBr_3$:Ce	30 ± 9.3
$LaCl_3$:Ce	45 ±16.4
BGO	28 ± 8

In this study, the response of three detectors: 3 x 3 (inches) lanthanum-halide ($LaBr_3$:Ce and $LaCl_3$:Ce) and 5 x 5 (inches) BGO, were tested for the detection of low energy prompt gamma-rays from boron contaminated water samples using a portable neutron generator model MP320 based KFUPM setup. The boron concentration was varied over 0.031, 0.125, 0.250 and 0.500 wt% in water samples. The experimental data were compared with the results of Monte Carlo simulations. The results of this study clearly show that, $LaBr_3$:Ce and $LaCl_3$:Ce detectors have excellent energy resolution to resolve boron low energy prompt gamma-rays from background prompt gamma-rays. The excellent agreement between the experimental yield of prompt gamma-rays with the calculated yield obtained by Monte Carlo simulations of prompt gamma-rays for the given concentration, shows the $LaBr_3$:Ce and $LaCl_3$:Ce detectors excellent performance in detecting low energy prompt gamma-rays. In spite the big deference in volumes between

BGO and lanthanum-halides ($LaCl_3$:Ce and $LaBr_3$:Ce) detectors, BGO is larger than lanthanum-halides by a factor of 4.63, lanthanum-halide detectors have comparable, MDC values of boron-contaminated water samples for KFUPM PGNAA setup. In addition, we observed that $LaBr_3$:Ce detector has lower MDC value of boron-contaminated water samples than $LaCl_3$:Ce detector for KFUPM PGNAA setup.

REFERENCES

[1] Richard J.C. Brown, Martin J.T. Milton. *Analytical techniques for trace element analysis: an overview*. Trends in Analytical Chemistry, Vol. 24, No. 3, 2005

[2] Ronald L. Bishop and M. James Blackman, *Instrumental Neutron Activation Analysis of Archaeological Ceramics: Scale and Interpretation*. Acc. Chem. Res., 2002**,** 35 (8), pp 603–610}

[3] C.W.E. van Eijka, P. Dorenbos, E.V.D. van Loef, K. Kramer, H.U. G,udel. *Energy resolution of some new inorganic-scintillator gamma-ray detectors*. Radiation Measurements 33 (2001) 521–525

[4] Alain Iltis, M.R. Mayhugh, P. Menge, C.M. Rozsa, O. Selles, V. Solovyev. *Lanthanum halide scintillators: Properties and applications.* Nuclear Instruments and Methods in Physics Research A 563 (2006) 359–363

[5] F. Quarati, A.J.J. Bos, S. Brandenburg, C. Dathy, P. Dorenbos, S. Kraft,R.W. Ostendorf, V. Ouspenski, Alan Owens. *X-ray and gamma-ray response of a 2'' x 2'' LaBr3:Ce scintillation detector.* Nuclear Instruments and Methods in Physics Research A 574 (2007) 115–120

[6] B.D. Milbrath, B.J. Choate, J.E. Fast, W.K. Hensley, R.T. Kouzes, J.E. Schweppe. *Comparison of LaBr3:Ce and NAI(Tl) scintillators for radio isotope identification devices.* Nuclear Instruments and Methods in Physics Research A 572 (2007) 774–784

[7] M. Ciemala a, D.Balabanski, M.Csatlo, J.M.Daugas, G.Georgiev , J.Gulyas , M.Kmiecik, A.Krasznahorkay, S.Lalkovski, A.Lefebvre-Schuhl, R.Lozeva, A.Maj, A.Vitez. *Measurements ofhigh-energy g-rayswithLaBr3 : Ce detectors.* Nuclear Instruments and Methods in Physics Research A 608 (2009) 76–79.

[8] S. Normand, A. Iltis, F. Bernard, T. Domenech, P. Delacour. *Resistance to g irradiation of LaBr3:Ce and LaCl3:Ce single crystals.* Nuclear Instruments and Methods in Physics Research A 572 (2007) 754–759.

[9] R. Pania, P. Bennatia, M. Bettia, M.N. Cintia, R. Pellegrinia, M. Mattiolib, V. Orsolini Cencellic, F. Navarriad, D. Bollinid, G. Moschinie, F. Garibaldif, F. de Notaristefani; *Lanthanum scintillation crystals for gamma ray imaging;* Nuclear Instruments and Methods in Physics Research A 567 (2006) 294–297

[10] D. Alexiev, L. Mo, D. A. Prokopovich, , M. L. Smith, and M. Matuchova; *Comparison of $LaBr_3$: Ce and $LaCl_3$:Ce With NaI(Tl) and Cadmium Zinc Telluride (CZT) Detectors*. IEEE TRANSACTIONS ON NUCLEAR SCIENCE, VOL. 55, NO. 3, JUNE 200

[11] R.L. Paul, R.M. Lindstrom. *Prompt Gamma Neutron Activation Analysis: Fundamentals and Applications*. Radioanal.Nucl. Chem. 243 (2000) 181-189.

[12] H.-C. Mehnera, F. Simonellib ; *Wide energy range efficiency calibration for a lanthanum bromide scintillation detector.* Radiation Measurements 43 (2008) 506 – 509.

[13] Naqvi A. A., M. M. Nagadi and O. S. B. Al-Amoudi, *Elemental Analysis of Concrete Samples Using an Accelerator-based PGNAA Setup.* Nuclear Instruments & Methods in Physics Research B, Vol. 225/3 (2004) pp. 331-338.

[14] M. Maurshall, J. Oxley**.** *Aspects of Explosives Detection*, 2009, Elsevier.

[15] Brown, Douglas R.; Gozani, Tsahi, *Thermal neutron analysis technology*. Proc. SPIE Vol. 2936, p. 85-94, Physics-Based Technologies for the Detection of Contraband, Lyle O. Malotky; John J. Pennella; Eds.

[16] Khokhlov V.F. K.N.Zaitsev , V.N.Beliayev , V.N.Kulakov , A. A.Lipengolts; A. A. Portnov ; *Prompt gamma neutron activation analysis of ^{10}B and Gd in biological samples at the MEPhI reactor*. Applied Radiation and Isotopes, Vol. 67(2009) pp 251–253.

[17] P. S. Ramanjaneyulu,1 Y. S. Sayi,1 T. Newton Nathaniel, A. V. R. Reddy, K. L. Ramakumar. *Determination of boron in water samples by chemical prompt gamma neutron activation analysis*; Journal of Radioanalytical and Nuclear Chemistry, Vol. 273, No.2 (2007) 411–414.

[18] Abdel-Sabour, M.F ; Abdel-Haleem, A.S; Sorror, A ; Zohny, E ; *Investigation of water hyacinth samples by prompt gamma-ray neutron activation analysis. A comparison indication of pollution in Egyptian water bodies*; Environmental Protection Engineering , Volume 23, Issue 3-4, 1997, Pages X-11

[19] Yong Sam Chung, Jong Hwa Moon, Young Ju Chung, Kil Yong Lee, Yoon Yeol Yoon ; *Determination of toxic and trace elements in algae by instrumental neutron activation analysis*. Journal of Radioanalytical and Nuclear Chemistry, Vol. 240, No. 1 (1999) 95-100

[20] Z. Idiria,_, H. Mazroua, S. Beddeka, A. Amokraneb, A. Azbouchea. *Monte Carlo optimization of sample dimensions of an 241Am–Be source-based PGNAA setup for water rejects analysis*; Nuclear Instruments and Methods in Physics Research A 578 (2007) 279–288.

[21] Naqvi A. A. M. M. Nagadi, Khateeb-ur-Rehman, M. Maslehuddin and S. Kidwai. *Monte Carlo simulations for design of the KFUPM PGNAA facility*. Radiation Physics and Chemistry, Vol. 66 (2003) pp 89 – 98.

[22] Naqvi A.A., M. Maslehuddin , M.A. Garwan , M.M. Nagadi, O.S.B. Al-Amoudi M. Raashid , Khateeb-ur-Rehman. *Effect of silica fume addition on the PGNAA measurement of chlorine in concrete* ; Applied Radiation and Isotopes 68 (2010) 412–417.

[23] G.F. Knoll, *Radiation detection and measurements,* JohnWiley and Sons Inc., New York 2000.

[24] Kenneth S. Krane, *introductory nuclear physics*. John Wiley & Sons, 1988.

[25] A. Hamed and A. M. Hassan. *Estimation of Boron in some local materials by prompt gamma ray neutron activity analysis technique*. Proceedings of the 2nd Environmental Physics Conference 18-22 Feb. 2006, Alexandria, Egypt.

[26] A. Favalli, H-C. Mehner, V. Ciriello, B. Pedersen. *Investigation of the PGNAA using the LaBr3 scintillation detector.* Applied Radiation and Isotopes 68 (2010) 901–904.

[27] A. Favalli, H.-C. Mehner, F. Simonelli. *Wide energy range efficiency calibration for a lanthanum bromide scintillation detector.* Radiation Measurements 43 (2008) 506 – 509.

[28] T. Martinez, D. Cana-Ott, and C. Guerrero. *Test of a 3"x3" LaCI3:Ce crystal and neutron sensitivity of lanthanum halide scintillators.* 2008 IEEE Nuclear Science Symposium Conference Record, N02-403.

[29] E. H. Seabury, J. C. Wharton, A. J. Caffrey. Response of a LaBr3(Ce) Detector to 2-11 MeV Gamma Rays. IEEE Nuclear Science Symposium (2006).

[30] John E. McFee, Anthony A. Faust, H. Robert Andrews, Vitaly Kovaltchouk, Edward T. Clifford, and Harry Ing. *A Comparison of Fast Inorganic Scintillators for Thermal Neutron Analysis Landmine Detection.* IEEE TRANSACTIONS ON NUCLEAR SCIENCE, VOL. 56, NO. 3, JUNE 2009.

[31] F. De Corte, A. Aimonits, A. De Wispelaere, J. Hoste, *Accuracy and Applicability of the ko-standardization Method*. Radioanal. Nucl. Chem. 113 (1987) 145-161.

[32] R. M. Lindstrom, R.F. Fleming, R. L. Paul, E. A. Mackey. *The ko Approach in Cold-neut from Prompt-gamma Activation Analysis*, Proc. Int. KO Users Workshop (F.De Corte, Editor) Universities Gent, Gent (1992) 121-124.

[33] IAEA. Final report of coordinated research project. *Database of prompt Gamma Rays from Slow Neutron Capture for Elemental Analysis*. International Atomic Energy Agency, Vienna, 2006.

[34] T.B. Ryves, E.B. Paul, *The Construction and Calibration of a Standard Thermal Neutron Flux Facility at the National Physical Laboratory*, J. Nucl. Energy 22 (1968) 759-775.

[35] Norman E. Holden. *Temperature dependence of the Westcott g-factor for capture and neutron fission reactions in ENDF/B.* High Flux Beam Reactor Division Brook haven National Laboratory Upton, New York 1973 USA (516) 282-5204.

[36] A. M. Lone, S. F. Mughabghab, R. Paviotti-Corcuera, *Development of a Database for Prompt –ray Neutron Activation Analysis*, Summary report of second IAEA Research coordination Meeting, INDC (NDS)-424, Vienna, Austria (2001) 85-92.

[37] Briesmeister J. F. (Ed). *MCNP4B2 –A General Monte Carlo N-Particles Transport Code.* Los Alamos National Laboratory Report, LA-12625. Version 4A. Los Alamos National Laboratory Report, LA-12625-M, 1997.

[38] Olivera, C., Salgado, J. Gonclves, I.F., Carvalho, F.G. and Leitao, *A Monte Carlo Study of the Influence of the Geometry Arrangements and Structural Materials on a PGNAA System Performance fore Cement Raw Material Analysis*. Applied Radiation Isotopes, Vol. 48 (1997 b) pp 1349-1354.

[39] Olivera, C., Salgado, J. and Carvalho, F.G. *Optimization of PGNAA instrument design for cement raw materials using the MCNP code*. J. Radio. Chem., Vol. 216 (1997 a) pp 191-198.

[40] Howell, S.L., Sigg, R.A., Moore, F.S. , DeVol, T.A. ; *Calibration and validation of a Monte Carlo model for PGNAA of chlorine in soil*. Journal of Radioanalytical and Nuclear Chemistry , Vol. 244, (2000) , pp. 173-178.

[41] Idiri, Z. Mazrou, H. Amokrane, A. , Bedek, S.; *Characterization of an Am-Be PGNAA set-up developed for in situ liquid analysis: Application to domestic waste water and industrial liquid effluents analysis;* Nuclear Instruments and Methods in Physics Research, Section B: Beam Interactions with Materials and Atoms , Vol. 268, (2010) , pp.213-218**.**

[42] A.A. Naqvi, **M.S.Al-Anezi**, ZameerKalakada, A.A.Isab, M.Raashid, Khateeb-ur-Rehman, F.Z. Khiari, M.A.Garwan, O.S.B.Al-Amoudi ,M.Maslehuddin. *Detection efficiency of low levels of boron and cadmium with a LaBr3:Ce scintillation detector.* Nuclear Instruments and Methods in Physics Research, section A 665 (2011) 74-79.

[43] A.A. Naqvi, ZameerKalakada, **M.S.Al-Anezi**, M.Raashid, Khateeb-ur-Rehman, M. Maslehuddin, M.A.Garwan (2011). *Low energy prompt gamma-ray tests of a large volume BGO detector.* Applied Radiation and Isotopes 70 (2012) 222–226.

[44] A.A. Naqvi, ZameerKalakada, **M.S.Al-Anezi**, Faris. A. Al-Matouq , M.Raashid, Khateeb-ur-Rehman, M. Maslehuddin. *Response tests of a LaCl3:Ce scintillation detector with Low energy prompt Gamma Rays from Boron and Cadmium*. Applied Radiation and Isotopes 70(2012) 882–887.

[45] Thermo Scientific Company, [www.thermoscientific.com].

[46] H. Vincke, E. Gschwendtner, C.W. Fabjan, T. Otto. *Response of a BGO detector to photon and neutron sources: simulations and measurements.* Nuclear Instruments and Methods in Physics Research A 484 (2002) pp.102–110.

[47] Gerhart C. Lowenthal,P. L. Airey. *Practical applications of radioactivity and nuclear radiations an introductory text for engineers, scientists, teachers and students*. Cambridge university press, 2001.

[48] Choi H.D., R.B. Firestone, R.M. Lindstrom, G.L. Molnar; S.F. Mughabghab; R. Paviotti-Corcuera, Zs. Revay; A. Trkov and C.M. Zhou (2006). *Database of Prompt Gamma-Rays from Slow Neutron Capture for Elemental Analysis*, International Atomic Energy Agency, Vienna.

[49] A.A. Naqvi, M.Maslehuddin, M.A.Garwan, M.M.Nagadi, O.S.B.Al-Amoudi, M. Raashid, Khateeb-ur-Rehman. *Effect of silica fume addition on the PGNAA measurement of chlorine in concrete.* Applied Radiation and Isotopes 68 (2010) 412–417.

[50] C. Michael Lederer. *Table of Isotopes*, seven edition. John Wiley & Sons.

[51] R. F. Christy. *The coupling of angular momenta in nuclear reactions*. Physics Review, Volume 89, Number 4, 1953.

[52] Triangle Universities Nuclear Laboratory (TUNL), [www.tunl.duke.edu].

VITAE

- Mohammad Saleh Al-Anezi
- Nationality: Saudi, Age: 32
- Permanent address: National Center For Mathematics and Physics, King Abdulaziz City for Science and Technology, P.O.Box 6086, Riyadh 11442, Saudi Arabia.
- Permanent E-Mail: malanazi@kacst.edu.sa
- Received B.Sc. in Physics from King Saud University (KSU), Riyadh, Saudi Arabia in June, 2004.
- Joined Physics Department, King Fahd University of Petroleum and Minerals as a full time student in August, 2007.
- Completed Master's degree requirements in Physics at King Fahd University of Petroleum and Minerals in July, 2012.